TÉCNICO LISBOA

Assessment of groundwater resources in an intensively irrigated area in Golegã, Portugal

Analysis of the impact of climate change and adaptation measures

Akram Hisham Ali Mohamed

Thesis to obtain the Master of Science Degree in

Environmental Engineering

Supervisor:

Luís Filipe Tavares Ribeiro

Co-supervisors:

Maria Paula Sofio Silva Mendes

Examination Committee

Helena Maria Rodrigues Vasconcelos Pinheiro (President)

Luís Filipe Tavares Ribeiro

Maria Teresa Condesso de Melo

November 2018


GroundwatCH
Groundwater / Global Change

TÉCNICO
LISBOA

TECHNISCHE
UNIVERSITÄT
DRESDEN

UNESCO-IHE
Institute for Water Education

Assessment of groundwater resources in an intensively irrigated area in Golegã, Portugal

Analysis of the impact of climate change and adaptation measures

Master of Science Thesis
by
Akram Hisham Ali Mohamed

Supervisor
Luís Filipe Tavares Ribeiro

Mentors
Maria Paula Sofio Silva Mendes

Examination committee
Helena Maria Rodrigues Vasconcelos Pinheiro (President)
Luís Filipe Tavares Ribeiro
Maria Teresa Condesso de Melo

This thesis is submitted in partial fulfillment of the requirements for the academic degree of

Master of Science in Water Science and Engineering
UNESCO-IHE Institute for Water Education, Delft, the Netherlands

Master of Science in Environmental Engineering
Instituto Superior Técnico, Universidade de Lisboa, Portugal

Master of Science in Hydro-Science and Engineering
Technische Universität Dresden, Germany

MSc research host institution
Instituto Superior Técnico, Universidade de Lisboa, Portugal

November 2018

Acknowledgment

A special gratitude to my supervisor Luis Ribeiro and my mentor and co-supervisor Maria Paula Mendes for the continuous support and guidance throughout the past months. Without your patience and constant push forwards, I wouldn't have been able to see the light at the end of this tunnel. You have offered constructive feedback and gave an expert opinion on all the research issues that I have faced during this project.

To Mr. Filipe Miguéns, thank you for providing all your expertise to make my modeling experience using GMS as smooth as possible. And to Dr. Hans Van der Kwast from IHE-Delft, a special thank you for making me believe in a world of freely shared knowledge and open source software. The guidance of your QGIS online course has been a great support during this research work.

To my newly formed family here in Europe and across the world, thank you for all the support and inspiration during the whole term of the program. I am grateful to each and every one of you who have shared his personal and/or professional experience whenever it was needed to inspire or guide me through this journey of ours. These memories have always pushed me forward whenever the mission seemed impossible. A special thanks to Mr. Manuel Duarte de Sousa, my dearest friend from Portugal, for your continuous motivation and support.

Finally, to my family back home in Egypt for being my backbone at all times. My mother and father, without you I wouldn't have made it. Your consistent support and inspiration have kept me going.

To my grandfather, Dr. Abdu Shata, the most inspirational person I have ever met in my life, I am most grateful to you to have raised my curiosity towards earth sciences and especially groundwater studies. You have always pushed me to be better as a human being. I can't find better words to describe your support but those fine word wrote by my cousin:

"He has achieved success who has lived well, laughed often and loved much; who has gained the respect of intelligent men and the love of little children; who has left the world better than he found it; who has never lacked appreciation of earth's beauty or failed to express it; who has always looked for the best in others and given them the best he had; whose life was an inspiration; whose memory a benediction. In the loving memory of my beloved grandfather, what you left behind was woven into our lives."

This thesis was developed in CERIS - CIVIL ENGINEERING RESEARCH AND INNOVATION FOR SUSTAINABILITY, a research center of Instituto Superior Técnico of Lisbon in the context of the R&D activities of the group Hydrogeology and Geosystems.

Resumo

A água de superfície sempre foi a principal fonte de água para as culturas irrigadas nas proximidades de grandes rios, mas a segurança do abastecimento de água de superfície é comprometida pela variabilidade climática, intervenção humana pela construção de reservatórios e contaminação por poluentes antropogênicos ou naturais. Assim, a dependência das águas subterrâneas como fonte mais segura de água para irrigação tem aumentado significativamente, especialmente durante os anos de seca. O rio Tejo tem uma grande importância socioeconômica para Portugal. Na área de Golegã, o sistema aquífero aluvial Tejo-Sado é usado para garantir as necessidades de água nas áreas urbanas e agrícolas intensivas. O milho como principal cultura da região tem um consumo muito alto e a área está passando por uma série de períodos de seca que comprometem o balanço hídrico entre o sistema aqüífero e os rios adjacentes.

Sabe-se que existe uma interação entre o sistema aqüífero Tejo-Sado e os corpos de águas superficiais ao seu redor, o que suscita preocupações não apenas sobre o esgotamento das águas subterrâneas, mas também afeta o fluxo ecológico nos dois rios. Uma investigação da recarga e do fluxo de águas subterrâneas é o principal objetivo deste estudo. Dados de evapotranspiração detectados remotamente, que são verificados por medidas do solo, foram usados para avaliar a distribuição espacial da recarga de água subterrânea, dependendo do gradiente superficial do solo e da cobertura do solo. Um software de modelagem de águas subterrâneas baseado no MODFLOW, GMS, foi usado para avaliar quantitativamente a interação entre o subsistema aquífero aluvial Tejo-Sado e os rios Tejo e Almonda. Se uma interação significativa for detectada, isso significa que a taxa de extração e o tipo de cultura podem afetar fortemente os regimes de vazão dos rios de maneira indireta. Cenários de mudança no tipo de cultura, bem como projeções de mudanças climáticas que afetam a recarga, são então avaliadas.

Os resultados deste estudo confirmam a forte conexão entre a recarga do aqüífero aluvial Tejo-Sado e a diminuição da quantidade de precipitação em futuros cenários de mudanças climáticas. Essa diminuição nas taxas de recarga aumenta diretamente o rebaixamento devido à extração na área com distribuição densa do poço. A distribuição e o espaçamento dos poços de extração desempenham um papel muito importante no regime de vazão das águas subterrâneas e intensificam o efeito localmente. Mudar os tipos de culturas para vegetais em vez de milho, como cenário de adaptação, não foi conclusivo em termos de esgotamento das águas subterrâneas, embora tenha mostrado uma boa contribuição na diminuição do esgotamento do fluxo do rio no sistema aquífero aluvial.

Palavras-chave: Modelagem de águas subterrâneas, Interação rio-água subterrânea, MODFLOW, Recarga de águas subterrâneas, Aluviões Do Tejo, Alterações Climáticas

Abstract

Surface water has always been the main source of water for irrigated croplands in the proximity of big rivers, yet the security of the surface water supply is compromised by climate variability, human intervention by building reservoirs and contamination through anthropogenic or natural pollutants. Thus, dependency on groundwater as a safer source of irrigation water has been increasing significantly especially during drought years. The Tagus river holds a great socio-economic importance to Portugal. In the area of Golegã, the Tejo-Sado alluvial aquifer system is used to secure water needs by urban as well as intensive agricultural lands. Maize as the main crop in the area has a very high consumption and the area has been going through a series of drought periods that compromises the water balance between the aquifer system and the adjacent rivers.

It is known that there is an interaction between the Tejo-Sado aquifer system and the surface water bodies surrounding it which raises the concerns not only of groundwater depletion but also affecting the ecologic flow in both rivers. An investigation of the groundwater recharge and groundwater flow is the main objectives of this study. Remotely sensed evapotranspiration data, that is verified by ground measures, was used to evaluate the spatial distribution of the groundwater recharge depending on the surface ground gradient as well as land cover. A MODFLOW based groundwater modeling software, GMS, was then used to quantitatively assess the interaction between the Tejo-Sado alluvial aquifer subsystem and both the Tagus and Almonda rivers. If a significant interaction is detected, this means that extraction rate and crop type can strongly affect the flow regimes of the rivers in an indirect way. Scenarios of change in crop type, as well as climate change projections affecting recharge, are then assessed.

The results of this study confirm the strong connection between the recharge of the Tejo-Sado alluvial aquifer and the decrease in precipitation amounts in future climate change scenarios. This decrease in recharge rates directly increases the drawdown due to extraction in the area with dense well distribution. Extraction wells distribution and spacing plays a very important role in the groundwater flow regime and intensifies the effect locally. Changing crop types to vegetables instead of maize, as an adaptation scenario, was not conclusive in terms of groundwater depletion although it has shown a good contribution in decreasing the river flow depletion into the alluvial aquifer system.

Keywords: Groundwater Modeling, River-Groundwater Interaction, MODFLOW, Groundwater Recharge, Tejo-Sado Alluvial Aquifer, Climate Change

Abbreviations

APA	Agência Portuguesa do Ambiente
ARH	Administração Da Região Hidrografica Do Tejo
DEM	Digital Elevation Model
ET	Evapotranspiration
ETR	Real Evapotranspiration
EU	European Union
FAO	Food and Agriculture Organization of the United Nations
GHG	Greenhouse Gas
GMS	Groundwater Modeling Software
masl	Meters above Sea Level
MODIS	The Moderate Resolution Imaging Spectroradiometer
NSE	Nash–Sutcliffe Efficiency Coefficient
PDI	Palmer Drought Index
PET	Potential Evapotranspiration
QGIS	Quantum Geographic Information System
SNIRH	Sistema Nacional de Informação de Recursos Hídricos
SPEI	Standerdized Precipitation Evapotranspiration Index
SPI	Standardized Precipitation Index
SSD	Sun of Squared Difference
UNESCO	United Nations Educational, Scientific and Cultural Organization
USGS	United States Geological Survey

Contents

List of Figures

List of Tables

1 Introduction

1.1 General Introduction

The fluctuation in climate conditions and the increase of awareness regarding climate change influences on the future of our planet have made it clear to all nations that there is an urge to better understand and manage our resources to guarantee the sustainability of life on Earth. Scientific evidence has prominently proved that anthropogenic emissions of GHGs are having a noticeable effect on Earth's climate. This implies the urge to act upon and work on adaptation schemes for a more sustainably managed resource such as water resource.

The extreme droughts that have been hitting several regions around the world have caused a huge reduction on the surface water resources. This increased the dependency on the groundwater resource even in areas that were always depending on surface water for decades. Figure 1 shows the change in the recurrence of 100 years drought events in the European continent. Increasing population and expansion of irrigated agricultural areas along with the expanding economic development are also drivers of the water demand worldwide.

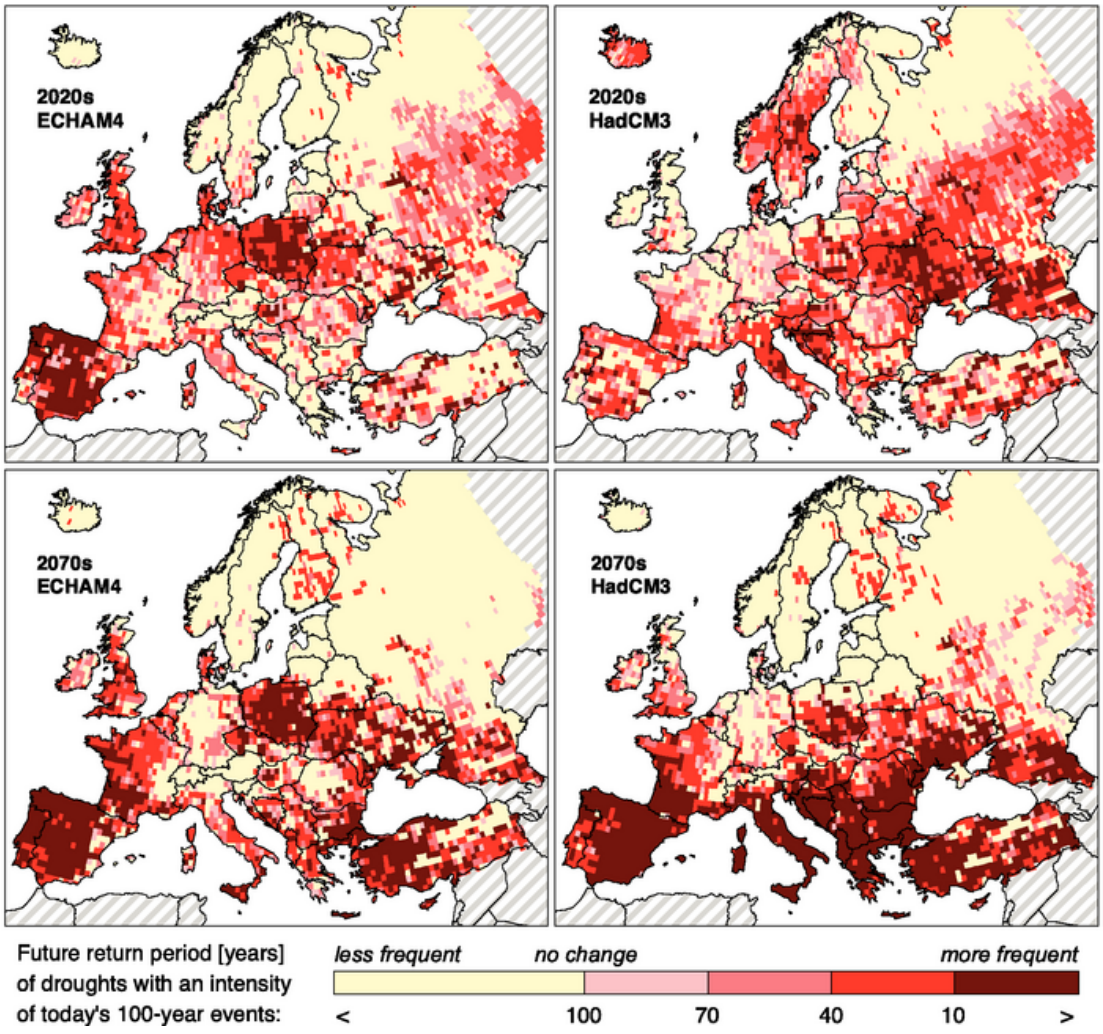

Figure 1: Change in the recurrence of 100 years drought (Ipcc, 2007)

Groundwater safe yield depends not only on hydrogeological factors but also on physical geographical and human-induced factors that are dependent on changes in water consumption and the resulting changes in groundwater recharge, quality and abstraction rates (Zektser and Everett, 2004).

Approximately one-fifth of the current world water demands for all different uses is provided by groundwater supply. The main water exploiters are irrigated agriculture, domestic potable water supply and industrial users (Zektser and Everett, 2004). From the year 2002 till 2012, agriculture accounted for 36% of the total water use in Europe, 75% of which is contributed to the Mediterranean region, where crop irrigated agriculture is extensively growing (EEA, 2016).

The EU Water Framework Directive adopted in October 2000, aimed at providing "good status" for surface water bodies and groundwater by 2015. Although not all target objectives were met, a second management cycle is supposed to end in 2021 and a third cycle ending at 2027, which is the new deadline for meeting the objectives. A Groundwater daughter directive recognizes that groundwater is a valuable natural resource and as such should be protected from deterioration and chemical pollution, taking in consideration the qualitative as well as the quantitative aspects (European Union, 2006).

This study was carried out in Portugal, specifically on the shallow alluvial aquifer of the Tagus river basin. The Tagus river runs through Spain and Portugal with an average discharge of 600 m^3/s and average annual volume of 19 km^3. Around 66% of the water is generated in Spain "upstream", while only 34% is generated in Portugal (Cordovil *et al.*, 2018). Although there are a lot of agreements and management cooperation of the river basin between the two countries, yet the increased intensity of droughts over the years have made it a difficult management task.

1.2 Problem Statement & Research Questions

The main problem tackled in this study is the depletion of groundwater resources in intensively irrigated areas under uncertain drought conditions. Exploitation of groundwater, especially by the irrigated agriculture sector, has been noticeably increasing for the past decades. This is due to the increasing risks from droughts that affect surface water scarcity. This makes land business owners depend more on the safer groundwater resource that is thought to be endless. Unfortunately, due to the lack of awareness towards groundwater resource management practice, these owners tend to abuse the groundwater resource not knowing that these drought events have also a less significant effect on groundwater, at least on the short term due to its the buffering capacity, but on the long term it affects the recharge patterns of the water resource.

Groundwater flow modeling has been widely used by research groups as well as management institutions to characterize the aquifer systems to help design good management schemes for resource sustainably. This is the method that was used in this case study in an agricultural area in central-west of Portugal, where it used to be dependent on surface water resource, namely the Tagus river, and now is deviating towards groundwater abstraction for irrigation. This is the first attempt of modeling the groundwater flow regime on such small scale in the area and will help

understand the interaction between groundwater and surface water resources and assess the risk of overexploitation under future climate change and crop type change scenarios.

Such problem provokes finding answers to the following research questions to better guide this thesis research work:

- What is the quantity of recharge that contributes to the groundwater storage in a normal year, and the effect of climate change on recharge?
- What is the effect of water abstraction from the shallow alluvial aquifer of the Tagus system for irrigation agriculture on the groundwater flow regime?
- What is the hydrodynamics of the surface water-groundwater interaction in terms of recharge and/or discharge?
- Is the current agriculture plot management the best for groundwater allocation?

1.3 Objectives

The objectives of this study are:

- Calculate recharge of the area of interest and its spatial distribution
- Groundwater-surface water interaction characterization
- Groundwater flow modeling at present and future climate change projections
- Assessment of adaptation measures to climate change

1.4 Thesis Layout

This thesis is organized in five main chapters, where this first chapter provides a general overview of climate change and its relation to groundwater resources on a global scale. Describes the main exploitation sectors of groundwater and the EU efforts into a more sustainable management scheme.

Chapter 2: Study Area describes in detail the characteristics of the study area in terms of geography, geology, hydrogeological setting and role of agricultural practice in the area, with a focus on water current demands.

Chapter 3: Methodology describes the main methods used to find answers to the research questions and fulfill the objectives of this research. This includes the recharge calculation method and groundwater flow modeling software.

Chapter 4: Model Setup describes the different stages of the modeling process and the development of the groundwater flow model. This includes the conceptual and geological models as well as the initial reference scenario input data and assumptions

Chapter 5: Results & Discussion displays the results of the simulated groundwater flow model, including a discussion of the water budget under climate change conditions and adaptation measures.

Chapter 6: Conclusions and Recommendations

2 Study Area

2.1 General Description

The area of interest in this study is in the heart of Portugal in the former Ribatejo plain (Figure 2), which translates to Upper Tagus; in relation to Lisbon that lies at the mouth of the Tagus river. Since 1976 it has been associated with the district of Santarém. At the center of the study area lies the city of Golegã, also called “Capital do Cavalo” meaning the “Capital of horses” as it has been the site for the gathering of horse breeders since the 18th century. The city of Golegã has a population of 3,845 inhabitants as of 2011 (INE). Agriculture as the main economic driver of the settlement of this population and some agri-dependent industries associated. The total surface area of the study area is 66 km2.

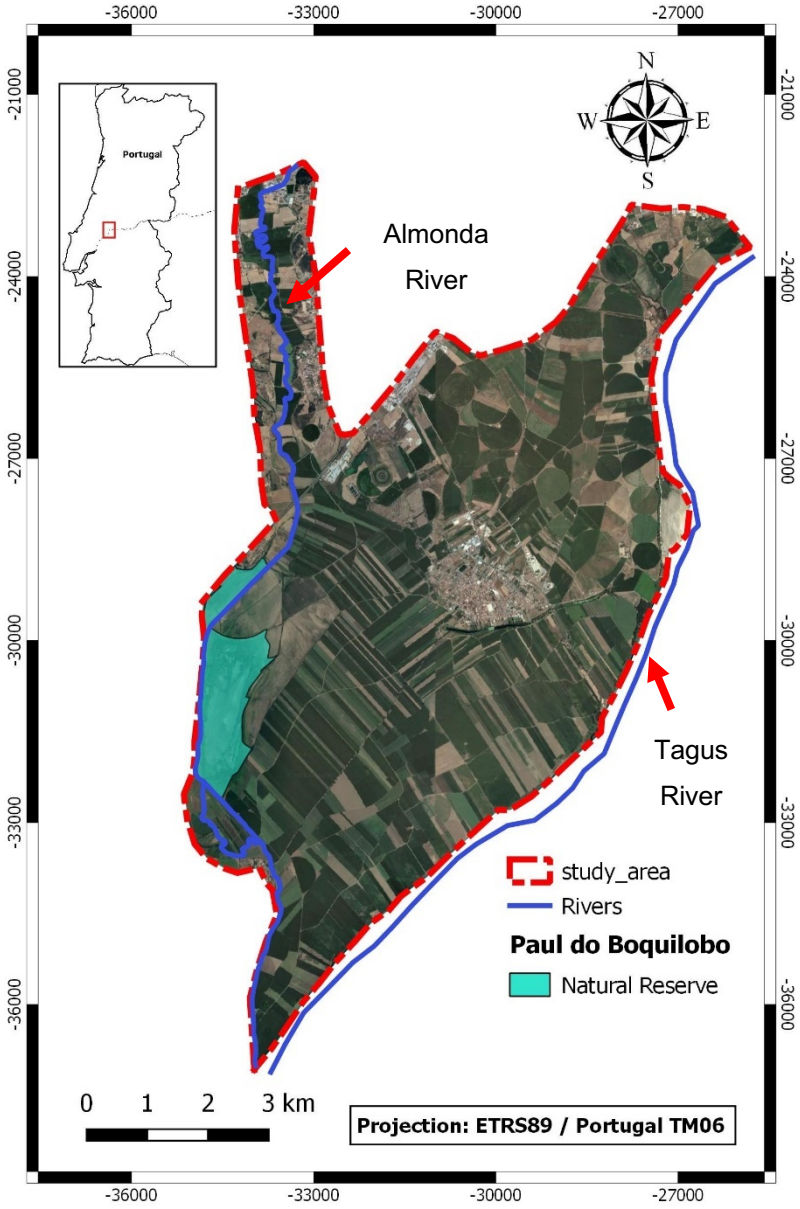

Figure 2: Location map

As seen in the topographic map in Figure 3, the area is mostly flat at the central and southern part and with higher gradients in the north and a very steep gradient in the arm in the northwestern part representing the valley where the river Almonda runs all the way until reaching the Tagus river. The highest elevation point within the study area is 62.6 masl, meters above sea level, while the lowest is 6.5 masl, yet the median value of the DEM is 17.5 masl, which means a very low elevation and a very low gradient in most of the area. The area is bounded by two main water bodies, the Almonda river from the west and the Tagus river from the east. This naturally water bounded system makes it very interesting to study the interactions between the different water bodies and the groundwater resource as well since the whole socio-economic setting of the area is mainly dependent on the water resources. Hence, a well-designed water resource management program and a sustainability plan of such important economic asset is a necessity.

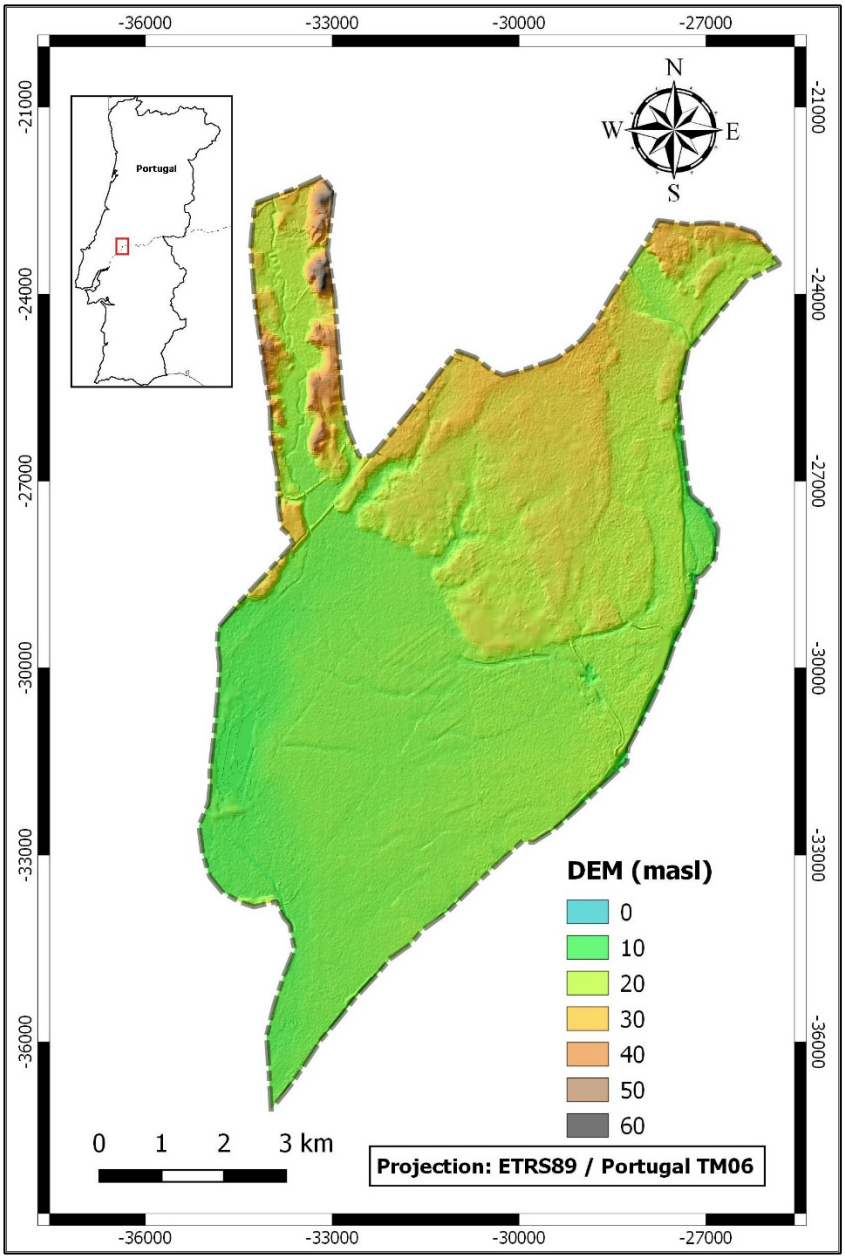

Figure 3: Topographic Map (Overlay of DEM & Hill Shade) in 2 m resolution

One more interesting and equally important feature to study in the area is the Paul do Boquilobo biosphere reserve which occupied an area of 554 ha (AGROTEJO, 2006). It has been classified by UNESCO as a biosphere reserve since 1981. This reserve is subdivided into three different zones according to critical preservation need. The nuclear zone is under total protection with limited accessibility for natural conservation and scientific research only. This zone also has an important role in flood control during wet seasons and the storage of water for the summer. The buffer zone is defined to minimize the impact on the natural ecosystem and promoting quality of life of the population. It is mainly intended for forestry and pasture production but also includes flooded agriculture lands. The transition zone consists of agriculture lands in which land and water use consider the sustainability of the natural resources around. The agricultural products of this zone are considered of high quality as they are produced in a natural reserve area.

This study area was suggested and requested to be studied by the local agriculture association in the area which is called AGROTEJO. This is the agricultural union of the north of the Tagus valley region. They have shown interest in the study as there has not been an attempt before to model the groundwater resource on such small scale in the area.

2.2 Geological Setting

The Tagus river originates at an elevation of about 1,500 meters in Spain and with a length of 1,000 meters and a catchment area of 80,630 km^2. Average discharge near the mouth is 400 m^3/s, but the river is characterized by extreme seasonal and annual variability. The evolution of the Lower Tagus Valley in the late Quaternary is determined by a narrow continental shelf and a deep glacial incision, rapid post-glacial relative sea-level rise, a wave-protected setting, and a large fluvial sediment supply. Since the Pliocene–Early Pleistocene the area was lifted up to 200 m above present sea level, which resulted in a staircase of Pleistocene fluvial terraces, mainly located east of the river up to a 100 m above the Holocene floodplain (Vis and Kasse, 2009a).

Figure 4 shows the regional geology map of the area. The lithological units' origin is fluvial, alluvium (Holocene) and terraces (Pleistocene) and are characterized by irregularity and complexity of stratification. Alluvium deposits are generally sand and clays with intercalations of coarse sand and pebbles with thickness up to 40 meters. While terraces are composed of basal deposits of gravel and pebble followed by an interglacial complex of sand and clay.

Figure 5 shows a transverse cut to the direction of the Tagus Basin through the study area from NW to SE. It shows that in the western part, from Golegã to Almonda river, FU-6A and FU-6B facial units dominate which are mostly clay and silt units with no evidence of coarser material potentially aquifer type deposits. On the other hand, the eastern part, Golegã to the Tagus River, the facial unit FU-8 shows up with a maximum thickness of 14 meters followed by a succession of subtidal flat deposits (FU-3B) and fluvially influenced tidal channels of intercalated sandy loam and fine sand (FU-5B). At the bottom is a 6 meters thick high gradient fluvial channel and coarse and very coarse sand (FU-1B). This suggests that on the shallow part of the right bank of the

Tagus river, more aquifer prone units exist closer to the river bank and with an extent of 1.5 km away in the west direction.

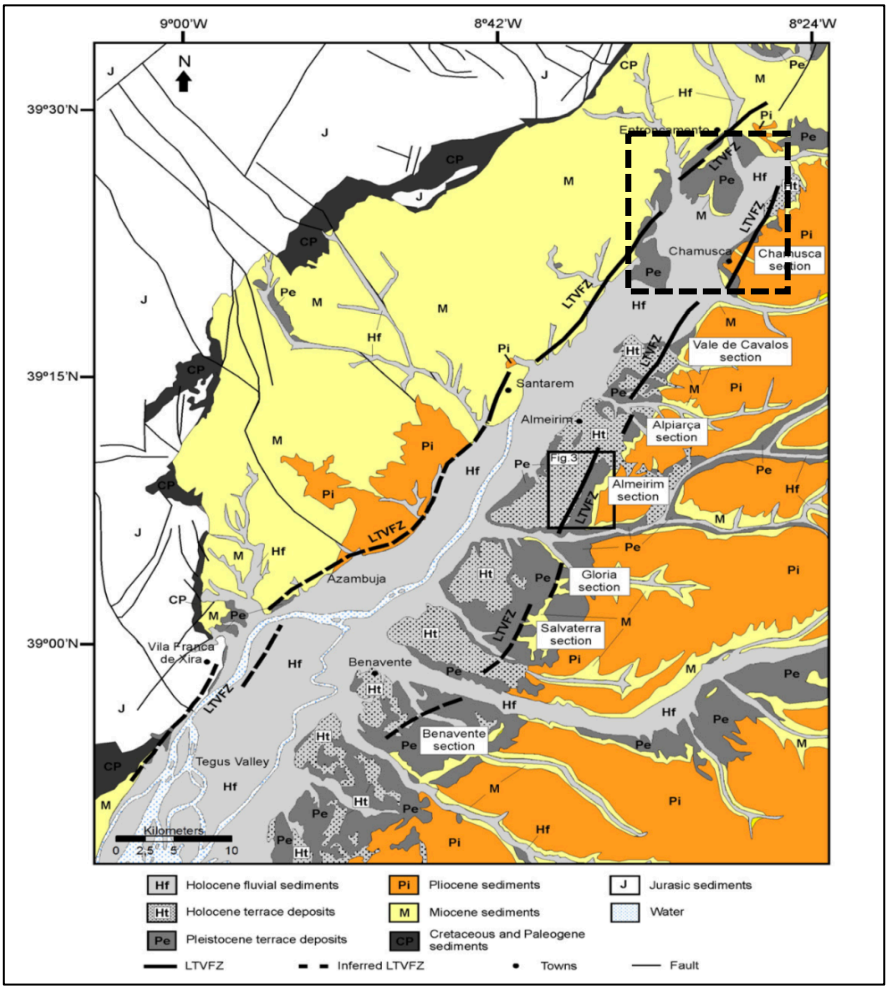

Figure 4: Regional Geology & Controlling Fault System (Study area in dotted square) (Canora *et al.*, 2015)

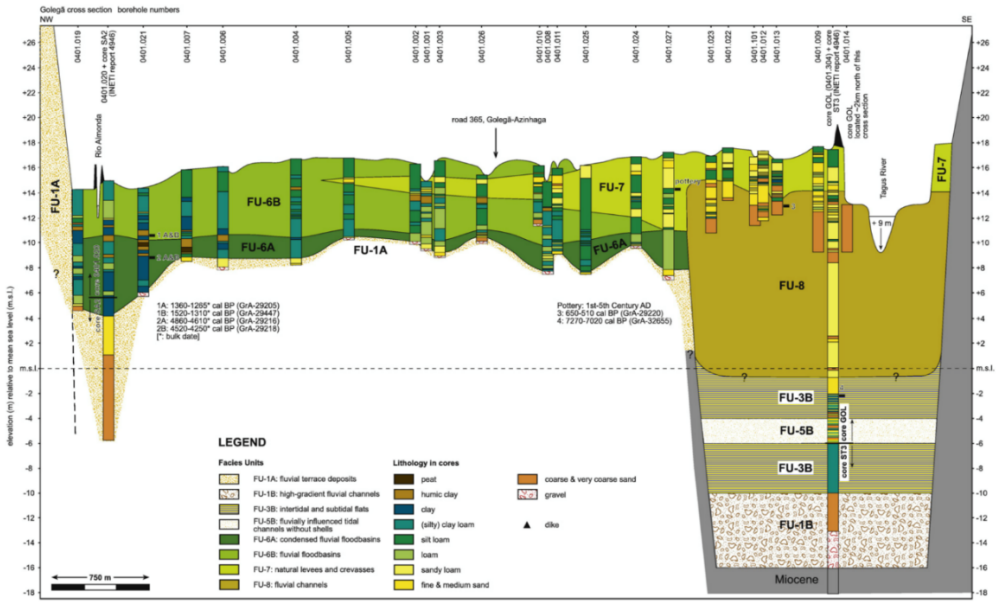

Figure 5: NE-SW cross-section through the study area (Vis and Kasse, 2009a)

2.3 Hydrogeological Setting

The Tejo-Sado alluvial aquifer system belongs to one of the most productive hydrogeological units of Portugal mainland; Tejo-Sado Miopliocenic multi-later aquifer system. The aquifer consists of alternating layers of fine and coarse sand or silty sandstone, clays, and silts. Sometimes intercalated with gravel. The base layer is composed of a layer of sand with gravel. The Almonda & Alviela tributaries can either recharge or discharge the alluvial aquifer system depending on the hydraulic potential (Mendes and Ribeiro, 2010).

The Tejo-Sado aquifer system is divided into three different sub-systems; the shallow and most recent alluvial aquifer subsystem, the right bank aquifer subsystem and the left bank aquifer subsystem. This study is concerned with the alluvial system as the agricultural sector in the area is mainly dependent on this system as it is the most economically efficient system for utilization. Figure 6 shows the extent of the Tejo-Sado alluvial aquifer subsystem within the limits of the study area along with the locations of the available data points. It indicates only one piezometric level monitoring well for this aquifer system within the area found on the database of SNIRH. During the field visit, 5 more wells were measured to be further used in the model calibration.

Within the study area and surrounding, 12 borehole log data points were provided by the Administração da Região Hidrografica Do Tejo (ARH Tejo). Figure 6 shows the spatial distribution of those borehole logs, indicating a higher density in the northern and southern parts of the study area and lower density in the central part with 3 to 5 meters separation.

The borehole records in Figure 7, provided by ARH Tejo, show that the main capture zone is in the sands and gravel layers of the alluvium and terraces as they have the highest transmissivity values. Generally, transmissivity increases from the margins towards the central part of the aquifer.

The hydrogeological units are represented in the gravel and sand layers which can allow water storage if the source exists. It is noted that the northern part is occupied by fine to coarse sand layers that decrease in thickness from west to east towards the Tagus river. On the other hand, layers of coarse gravel dominate in the southern part, which might indicate higher hydraulic conductivity, and decreases in thickness towards the river. An increase in the loose soil thickness is noticed in the southern part which is due to the flatness of the area leading to recent deposition of soil as well as the effect of intense agriculture practice. The bottom of the aquifer seems to be shallowing towards the south part where the Tagus and Almonda rivers meet, also showing a significant increase in the bottom clay layer underneath the aquifer. The significant change in thickness or the aquifer layers and the depth of the boreholes from west to east in the northern part is due to the topographic variation in surface elevation as seen in boreholes 144, 54 and 150, 149. The unit description and depths of the hydrological units are coinciding with the cross section produced by Vis and Kasse, 2009b.

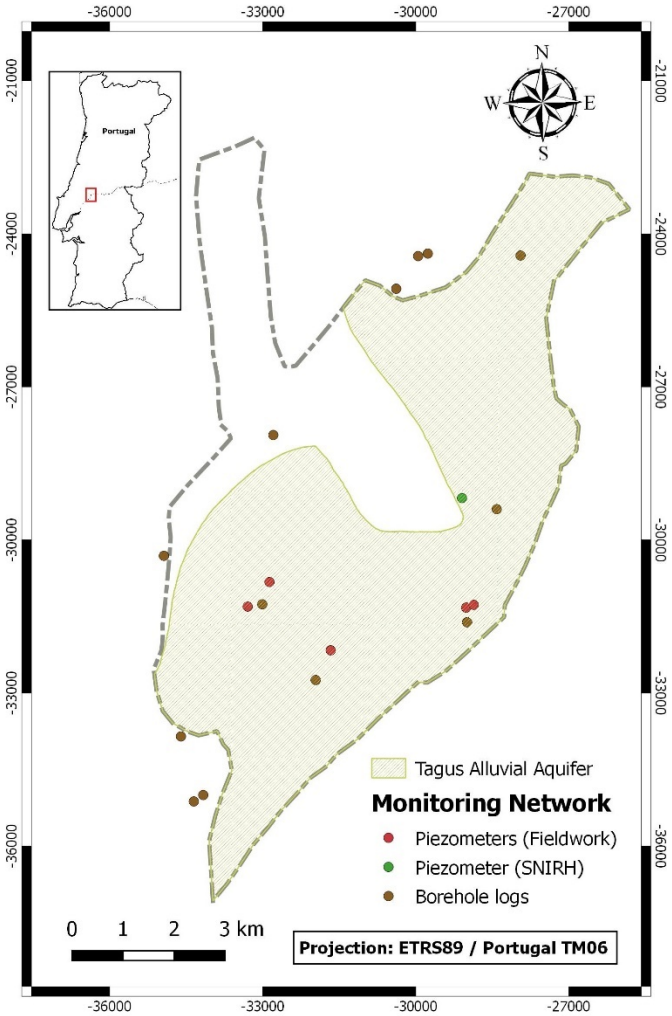

Figure 6: Tejo-Sado alluvial aquifer extent & Monitoring network

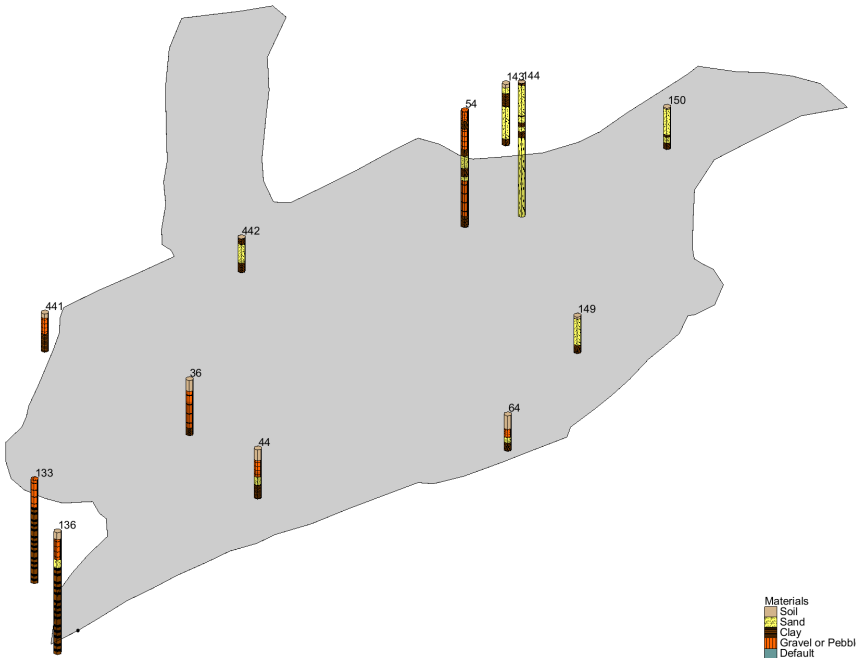

Figure 7: Borehole Logs location map (Z magnification of 20 times)

2.4 Agriculture

Agriculture is the primary economic sector in the region of Golegã as it is in a region of fertile soil, irrigated by two rivers, Tagus and Almonda. Agri-business is developed in the transition zone of the Paul do Boquilobo biosphere reserve according to the good agriculture practice. Agriculture lands cover 95% of the study area. The main crop type in the area is maize, occupying 90% of the land followed by 6% of vegetable production and 4% of vineyards, olive trees and some sunflower in the south near Azinhaga as shown in Figure 8.

The agricultural fields in the study area are set between two different configurations, either central pivotal sprinkler systems or narrow elongated fields parallel to each other with individual pumping wells. Each pivot has it's pumping well at the center. These pivotal systems are mainly located in the northern part of the area, north of the urban city of Golegã, while elongated fields are in the central and southern parts.

In 2007, a study in an unpublished report on an area of 11,713 ha that lies on the left bank of the Tagus river opposite to the study area, specifically in Pinheiro Grande and Carregueira, concludes that the annual agricultural crops occupy 66.6% in which maize occupies 80% and other vegetables like tomato, potato, and bell pepper occupy the other 20%. By including the efficiency of the irrigation systems, assuming 60% efficiency by furrow irrigation, 90% by drip irrigation and 85% by sprinklers, the total annual consumption was 1099 mm and 1204 mm by furrow irrigation of maize in an average year and critical year respectively. While on sprinkler systems, consumption is 776 mm and 850 mm in an average year and critical year respectively. As for all other crops, 675 mm and 769 mm of water are consumed per average year and critical year respectively, assuming drip irrigation systems.

To calculate the present actual consumption of the irrigated area, it was assumed that in the year 2007, the time when the report was made, 70% of the annual cultivated maize was irrigated by furrow irrigation systems. For calculating present time consumption, it was assumed that only 10% of the total annual cultivated maize is irrigated by furrow irrigation systems and the rest is irrigated by sprinkler systems. This results in a total annual consumption of 7,399,843 m3 of water by maize and 1,517,542 m^3 my other crops in an average year. Thus, the total annual consumption in an average year is 8,917,385 m^3 of water for an area of 11,713 ha.

Using the data from the previous study, the current consumption of irrigation in the study area, which has 6,660 ha of irrigated lands, is 40,010,959 m^3 per average year. This gives 109,619 m^3/day of groundwater pumping, assuming zero consumption by surface water.

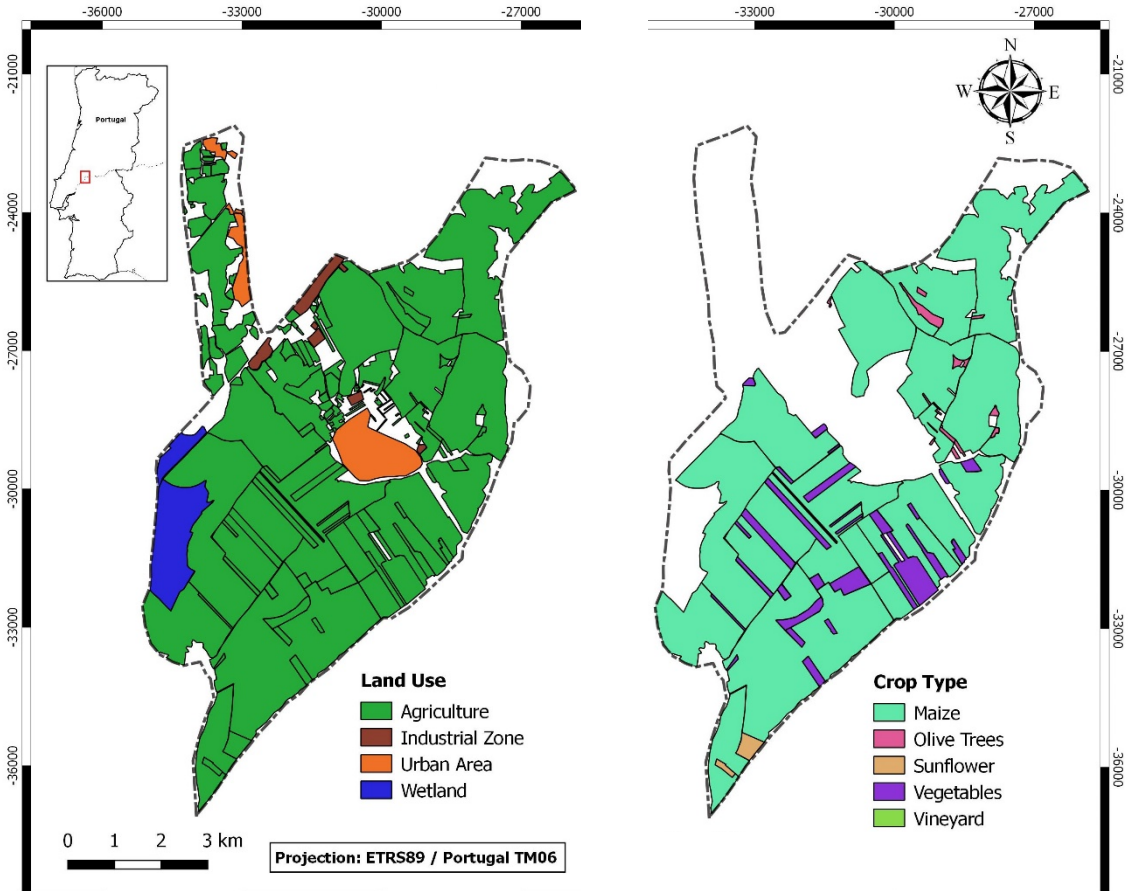

Figure 8: Land Use & Crop Type Maps

3 Methodology

3.1 Recharge Estimation

In the case of unconfined aquifers, when infiltration water reaches the capillary fringe, it displaces air in the soil and rock pores and causes the water table to rise. The time taken by the water infiltrating water to reach the initial water table level is a function of the thickness of the unsaturated zone and its vertical hydraulic conductivity. Usually, in lowlands and near the shoreline, where the unsaturated zone is thinner, recharge can reach the water table faster resulting in localized groundwater mounds (Fetter, 2001).

3.1.1 Drought Index & Time Interval Choice

To decide which time interval is to be modeled, a drought index was needed to be calculated as an indication of extreme drought and extreme wet years to be avoided for the model simulation. Several drought indices have been developed along the years and the most used ones are the Palmer drought index (PDI), Standardized Precipitation Index (SPI) and Standardized Precipitation Evapotranspiration Index (SPEI). According to Guttman, 1998, SPI is recommended as a drought index because it is simple, spatially consistent in interpretation probabilistic so can be used risk analysis and can be tailored to time periods of user's interest. While the PDI, on the other hand, is very complex, spatially variable and temporally fixed. According to Vicente-Serrano, Beguería and López-Moreno, 2010, SPEI is based on precipitation and temperature data and has the advantage of being multi-scalar in comparison to PDI, which is crucial in drought analysis. SPEI is like SPI calculation but includes the role of temperature variability effect on drought assessment.

Thus, SPEI was decided to be the best drought index to be used to choose a normal year within the past decade so that normal conditions would be modeled. A freely available software has been developed by Vicente-Serrano, Beguería and López-Moreno, 2010 to calculate the SPEI. SPEI was calculated using monthly precipitation and the potential evapotranspiration from the Thornthwaite method as input data. A simple water balance is then calculated as the difference between the precipitation and PET on a monthly time scale from the year 1989 till 2017. An accumulated time difference is calculated for a time series of 6 months. This measure the anomalies in the PT-PET values based on a comparison of observed total difference for an accumulated period of interest, 6-months in this case, with the long-term historical record of difference.

3.1.2 Real Evapotranspiration

Remotely sensed MODIS Global Terrestrial Evapotranspiration (ET) Product (NASA MOD16A2) was used. The MOD16 algorithm is based on the logic of the Penman-Monteith equation, which includes inputs of daily meteorological reanalysis data along with MODIS remotely sensed data products such as vegetation property dynamics, albedo, and land cover. This dataset is available

in 0.5 km spatial resolution. Running *et al.*, 2017 describes in detail the algorithm as shown in Figure 9.

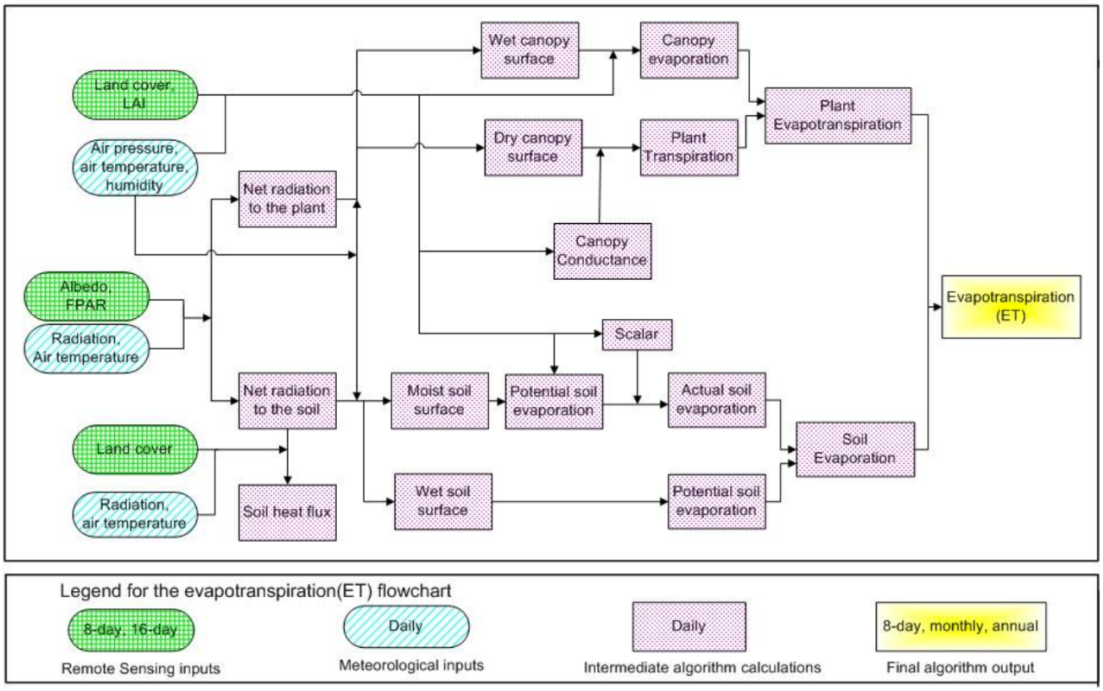

Figure 9: Flowchart of the improved MOD16 ET algorithm. LAI: leaf area index; FPAR: Fraction of Photosynthetically Active Radiation (Running *et al.*, 2017)

The pixel value of evapotranspiration is the sum of all eight days within the composite period. Due to the size of the raster datasets and for time constraints, only one raster was decided to be used as a representation of each month of the model time period. Initially, the accumulative raster of the first 8 days of the month was downloaded and processed for further calculation of the monthly evapotranspiration. But it was noticed that in some months, pixels of NODATA started appearing and it is associated with cloud cover at the time of remote sensing, especially that they coincided with the rainy season. Thus, all raster datasets of these months were downloaded and compared and the raster with the least number of NODATA available was used as a representative for the month.

The unit of evapotranspiration is given in kg/m^2 for an accumulation of 8 days, thus on a GIS-based platform, namely QGIS, calculations were done to transform the units from kg/m^2 to monthly cumulative in mm/day as in equation [1].

$$ETR_{Monthly\ Cumulative} = \frac{ETR_i * 1000}{1000 * 8} \times Number\ of\ days\ in\ the\ month \qquad [1]$$

3.1.3 Recharge Calculation

Finally, the recharge was calculated by subtracting the real evapotranspiration from the mean monthly precipitation values for each month and then added all together to give the total annual recharge in the study area.

3.2 Groundwater Flow Modeling

Groundwater flow models have been widely used for studying regional steady-state flow in aquifer systems; regional changes in the hydraulic head caused by changes in discharge or recharge (Fetter, 2001). Groundwater flow is controlled by the laws of physics and thermodynamics, and thus it can be described by differential equations. Flow is a function of variables described in partial differential equations in which x, y, and z represent the spatial coordinates and t as the time, all are independent variables.

According to Hubbert, 1940, the total potential energy acting upon groundwater indicated as force potential (Φ) is

$$\Phi = gz + \frac{P}{\rho} = gz + \frac{\rho g h_P}{\rho} = g(z + h_P) \quad [2]$$

Since $(z + h_P) = h$, the hydraulic head

Therefore, $\Phi = gh$

Where P is the pressure, ρ is the water density, z is the elevation component and h_p is the pressure head. Theoretically, the force potential is the driving force of the groundwater flow, while practically since gravitational acceleration is considered a contact everywhere on Earth, the hydraulic head h is a more convenient dimension to be used (Fetter, 2001).

Darcy's law is used to describe the relationship between the velocity vector and the hydraulic head gradient as in equation [3]:

$$q = -ki = -k \times \frac{\partial h}{\partial_{x,y,z}} \quad [3]$$

Where, q is the specific discharge that represents the velocity vector in the 3 components (X, Y, and Z), k is the hydraulic conductivity and I is the hydraulic gradient in the 3 components.

From the law of mass conservation, partial differential equations of the groundwater flow are derived. This law states that there can be no change in the net mass of the fluid in a small aquifer volume and that any change in this mass has to be compensated by a change in the mass flux out of that volume or a change in the mass stored in it, or both (Fetter, 2001). This equation in the steady state condition is as in equation [4]:

$$\frac{\partial q_x}{\partial x} + \frac{\partial q_y}{\partial y} + \frac{\partial q_z}{\partial z} = 0 \quad [4]$$

In steady state flow there is no change in the head with time and therefore time is not a dependent variable thus Laplace equation is used to combine Darcy's law and the law of mass conservation to describe the three-dimensional partial differential equation as in equation [5]:

$$\frac{\partial}{\partial x}(-k \times \frac{\partial h}{\partial x}) + \frac{\partial}{\partial y}(-k \times \frac{\partial h}{\partial y}) + \frac{\partial}{\partial z}(-k \times \frac{\partial h}{\partial z}) = 0 \quad [5]$$

For isotropic aquifers, where K is constant in all directions, Laplace equation becomes as in equation [6] and it is the governing equation for groundwater flow in homogeneous and isotropic aquifer system under steady-state conditions.

$$\frac{\partial^2 h}{\partial x^2} + \frac{\partial^2 h}{\partial y^2} + \frac{\partial^2 h}{\partial z^2} = 0 \qquad [6]$$

In case of the transient state, where variables are time-dependent, Laplace equation is modified to include the specific yield, which is the ratio of the volume of water that drains from a saturated rock owing to the attraction of gravity to the total volume of the rock. Equation [7] represent the deriving equation:

$$\frac{\partial^2 h}{\partial x^2} + \frac{\partial^2 h}{\partial y^2} + \frac{\partial^2 h}{\partial z^2} = \frac{S_y}{K}\frac{\partial h}{\partial t} \qquad [7]$$

In unconfined aquifers, water is derived from the storage by vertical drainage of water in the pore spaces resulting in a decline in the water table at extractions wells fields where water is pumped out for different water uses. Thus, the saturated thickness of the aquifer is subject to change with time and hence the ability of the aquifer to transmit water. Transmissivity, T, is the product of the hydraulic conductivity, K, and the saturated thickness, b, which is measured from the bottom of the aquifer to the water table level (T=Kb).

The solution of the equations of unconfined groundwater flow is very complicated for the fact of a changing water table with time. For this reason, and assuming a negligible vertical flow, the use of Dupuit assumptions to simplify the solution and these are:

- The hydraulic gradient is equal to the slope of the water table
- For small water table gradients, the streamlines are horizontal, and the equipotential lines are verticals; horizontal flow only
- Darcy's velocity is constant over the depth of flow, which is a function of the x component

Consequently, equation [8] is obtained:

$$Q = -Kh\frac{\partial h}{\partial x} \qquad [8]$$

Where Q is the groundwater flow, h is the piezometric head as well as the thickness of flow. Thus, by substituting in Boussinesq equation; the general flow equation for two-dimensional unconfined flow, equation [9] is obtained:

$$\frac{\partial}{\partial x}\left(h\frac{\partial h}{\partial x}\right) + \frac{\partial}{\partial y}\left(h\frac{\partial h}{\partial y}\right) = \frac{S_y}{K}\frac{\partial h}{\partial t} \qquad [9]$$

Where Sy is the specific yield. Due to the non-linearity of this equation, it is only solvable in very specific cases. For simplification and assuming a very small drawdown compared to the saturated aquifer thickness, the variable thickness, h, is replaced by an average thickness, b, assumed to be constant over the aquifer extent. As a result, the Boussinesq equation is linearized as in equation [10]:

$$\frac{\partial^2 h}{\partial x^2} + \frac{\partial^2 h}{\partial y^2} = \frac{S_y}{Kb} \frac{\partial h}{\partial t} \quad [10]$$

Most hydrogeologists would not develop a new method of solution for the flow equations or write new computer code for groundwater flow modeling. The USGS has published several computer models that are well tested and documented. Public domain is available free of cost for both mainframe and personal computers.

Freeze and Witherspoon, 1966 were the first to apply numerical models to simulate steady-state regional flow patterns in the hypothetical layered aquifer system. Application of groundwater flow models to large-scale aquifer system simulation started in 1978, with the Regional Aquifer-System Analysis (RASA) program of the U.S. Geological Survey. Computer-based numerical groundwater flow models used in most cases were the USGS MODFLOW, McDonald and Harbaugh, 1988, and USGS 3D finite difference model, Trescott, 1975. Significant advances in the regional flow system analysis were driven by the application of 3D groundwater flow models. The most widely used industrial groundwater modeling tool is MODFLOW since its release in 1988 (Zhou and Li, 2011).

MODFLOW is a block centered finite difference groundwater flow model. It only simulates saturated flow in a porous medium with uniform temperature and density. Modeled layers can be confined, unconfined or combined and it simulates recharge, evapotranspiration, areal recharge, flow to wells, flow to drains and flows through river beds (Fetter, 2001).

“Steady-state simulation has many applications in hydrologic investigations. It is used to analyze the natural (predevelopment) flow system as well as any new equilibrium conditions that have been attained during the course of development. Calibration of steady-state models provides information on hydraulic conductivity and transmissivity. Because storage effects are not involved in steady-state modeling, the results of steady-state calibrations are often less subject to ambiguity than those of transient- state calibrations. Steady-state analysis can also be a rapid method of evaluating new equilibrium conditions that may develop in response to future stresses.” (Franke, Reilly and Bennett, 1987).

The following section describes in more detail the 3D groundwater flow model inputs and development setup. For this study, Ground Water Modeling Software (GMS 10.3) was used to simulate the groundwater flow system to better understand the flow system performance under current conditions as well as interaction with surrounding surface water bodies. And then running several global change scenarios to be able to come up with adaptive solutions for the sustainability of water use in the area.

4 Model Setup

4.1 Conceptual Model

In studying a good groundwater flow system, the development of a conceptual model that is usually less complex than a real system is important (Fetter, 2001). Conceptual models are static and describe the present conditions of the system, further development of a dynamic numerical model is a must to predict future behavior.

The conceptual model describes the hydrogeological framework, groundwater flow, recharge, evapotranspiration, discharge to streams, water use and hydraulic properties of the alluvial aquifer system of the Tagus around the city of Golegã. The hydrogeological framework describes the physical dimensions and location of the aquifer. The boundaries of the alluvial aquifer within the study area were defined according to the limits defined by the Portuguese Environmental Agency (APA). This indicates a lateral contact between the alluvial aquifer and the deeper confined aquifer of the right bank of the Tagus river in the western part of the study area. According to Almeida *et al.*, 2000, there is an interaction between the two aquifer subsystems.

The top boundary of the model is the water table while the bottom boundary is considered a thick clay layer that separates it from the deeper confined aquifer. The contacts between the different hydrogeological units were determined based on the lithological description obtained from the drilled wells database in the region.

From the east and the south-western limits, the aquifer is bounded by the Tagus river and the Almonda river respectively. The interaction between both rivers and the aquifer system is among the most important aspects of this study. It is assumed that the groundwater flows toward the east from the high lands on the northwestern part and discharges in the Tagus river.

Recharge to the Tejo-Sado alluvial aquifer is mainly through infiltration of precipitation especially that most of the study area has a very low relief which makes runoff negligible. It is also believed that the Almonda river contributes to the aquifer from the west following the terrain relief. Evapotranspiration, on the other hand, contributes to the water budget where precipitation accumulates in flat lands which makes it easier to evaporate especially during the hot summer season. Another source of recharge is the inflow from the Tejo-Sado right bank aquifer subsystem, which is a very important component in the water budget.

Extraction wells primarily are for irrigation and domestic water supplies. This is the main external pressure on the aquifer system that needs to be well explored. The Paul Boquilobo ecological system lies in the south-western boundary of the study area along with the Almonda river. This is seen in the conceptual model as a discharge/recharge zone as there is a constant wetland/lake that should be interacting with the groundwater and contributing to the water budget.

4.2 Hydrogeological model

The first step towards the modeling objectives is to better understand the extent of the geological units within the study area thus the extent of the aquifer of interest. Since this study is focused on the Tejo-Sado alluvial aquifer, the model extent was modified to fit for the intersect between the alluvial aquifer and the study area. As a result, the northwestern part of the study area is not modeled as it belongs to the deeper Tejo-Sado right bank subsystem. Although there are an interaction and continuation between both aquifer subsystems, this is beyond the scope of this study.

Twelve borehole logs descriptions provided by the local Portuguese environmental body, ARH Tejo, were used to build the geological model. A software called GMS, Groundwater Modeling System was used for building the geological model. The software is developed by a US based company called AQUAVEO and a license provided by Instituto Superior Técnico was used.

The preliminary lithology correlation on cross sections showed a thick sequence of coarse sand and gravel layers intercalated with thin clay layers in the northern part of the area. This layer decreases in thickness in all directions and pinches out towards a finer sediment of sand closer to the river bank and towards the western edge of the aquifer. In the northern part, this layer's thickness ranges between 70 meters in the west and 20 meters at the river bank. In the southernmost part of the area, the same coarse gravel sediment appears with a much less thickness, around 20 meters, and pinches out towards the central south part into what is described as rock fragments, agglomerate and even limestone in boreholes 44 and 64. Knowing the geological background of the area as described in section 2.2, the existence of limestone from the Miocene age doesn't fit at such low depth.

After consulting with several experts of the depositional setting of the area and with a literature background, the layers of agglomerate, rock fragment and limestone were replaced to be equivalent to the gravel and pebble layer in the other boreholes. The result was much more consistent and fitted more within the lithological sequence.

Furthermore, the model was more simplified to match the level of detail of the groundwater characteristics in the aquifer. All sand and gravel layers were combined in one aquifer layer topped by a thin layer of soil in some areas and bounded by a clay layer at the bottom. Finally, a 3D model of the extent of the geological units was build using the function Solids in GMS software as shown in Figure 10.

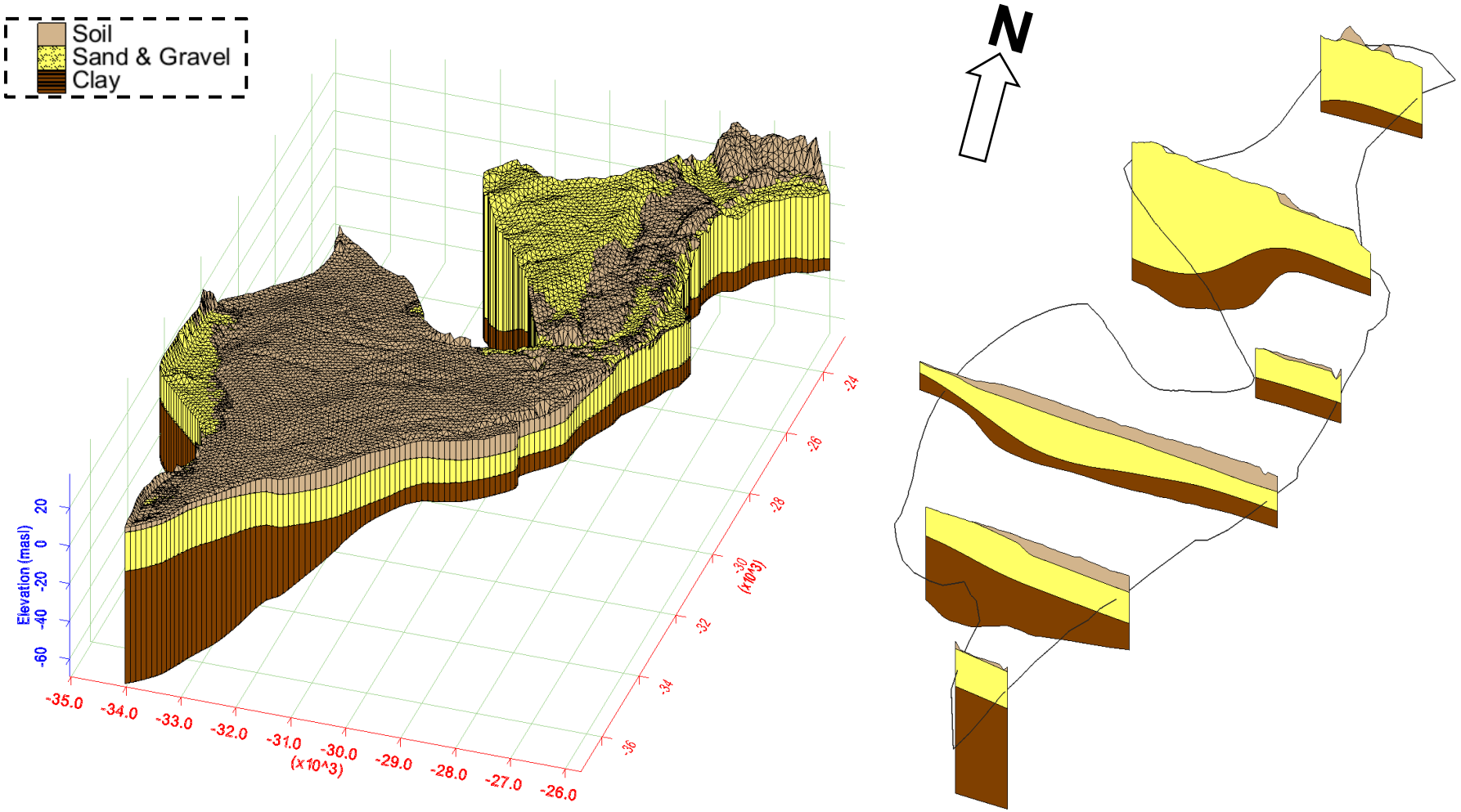

Figure 10: 3D Hydrogeological Model (Left) & Cross-sections showing variation in layers' thicknesses across the study area (Right)

4.3 Groundwater Flow Model

A steady-state model representing the hydrological year 2015/2016 was constructed to analyze the natural flow system as well as any new equilibrium conditions. A One-layer model was defined where the geological units of soil and the sand & gravel layer were combined. Because of the relatively small surface area of the study area and the high density of groundwater extraction, a discretization of 50 meters grid was used to simulate the groundwater flow and detect the small-scale movement. The main assumption that this model built upon is that the aquifer is assumed to be an isotropic unconfined aquifer. This means that the hydraulic properties of the aquifer are constant in all 3 directions.

4.3.1 Recharge

The closest climate monitoring station on the national system of Portugal (SNIRH) is Chamusca (39.3107° N, 8.3527° W). Due to the lack of climate datasets of the most important parameters like precipitation, temperature and wind speed from the year 2010 till 2015, a continuous dataset of monthly average precipitation and temperature from the year 1989 till 2014 from the SNIRH of the monitoring station of Vila Franca de Xira (38.9550° N, 8.9890° W). This city lies 80 Km downstream along the Tagus river from the study area. Further on, From the year 2015 till 2017, the dataset was acquired through the database of SNIRH, yet there were still missing data that was interpolated using a linear correlation of the dataset with the nearest monitoring station, Barragem de Magos. Figure 11 & Figure 12, shows the correlation curves of precipitation and temperature. Results show a root-mean-square value of 0.81 for precipitation data while temperature showed a value of 0.98. This show a very good correlation that makes this data reliable to use for the study area.

The difference in the climate data is due to the altitude difference between the two locations, as Vila Franca de Xira has an altitude of 1 masl while the study area lies at a median elevation of 17.5 masl. Also, it is at the northern edge of the Tagus Estuary where the wind system is probably different from the study area.

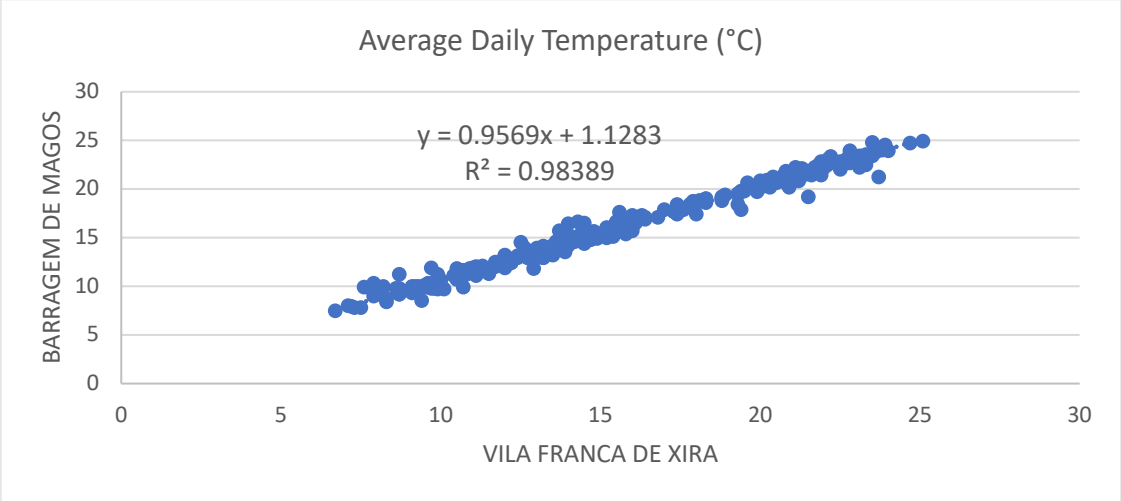

Figure 11: Temperature correlation

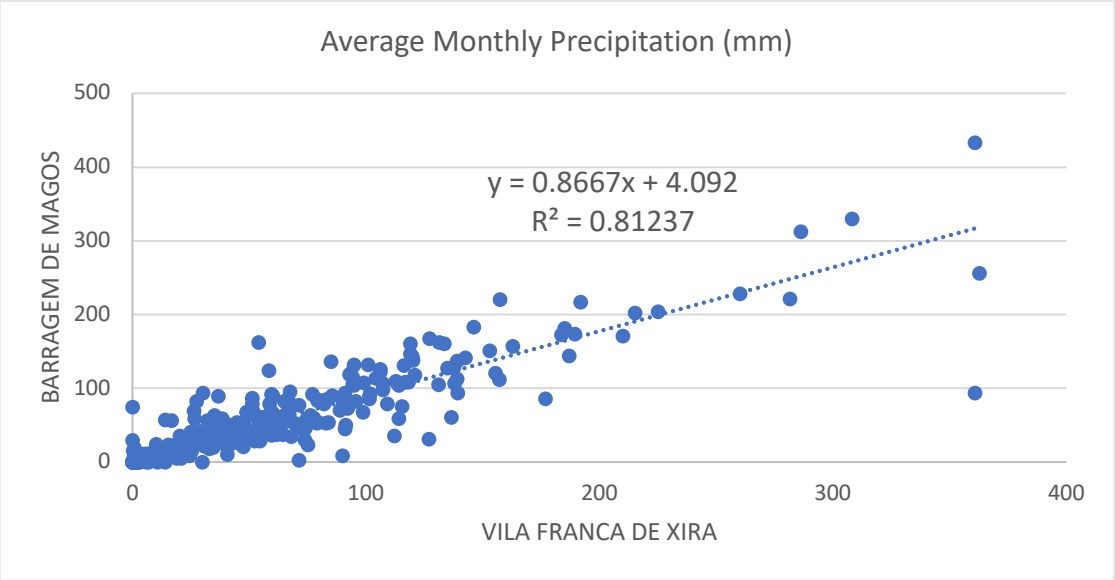

Figure 12: Precipitation correlation

Potential evapotranspiration (PET) was calculated using two different methods, Thornthwaite method, which relies only on temperature and latitude and the Penman-Monteith equation, which is much more complex as it involves solar radiation, wind speed and relative humidity in addition to temperature and latitude. On the other hand, remotely sensed real evapotranspiration data was used.

The top boundary is imported as a recharge package where the raster product from the recharge estimation section was used to assign recharge values for each model cell. These values are the difference between precipitation and real evapotranspiration.

4.3.2 Boundary Conditions

As described in seen in Figure 13, the aquifer with the study area is bounded from the eastern boundary by the Tagus river and from the southwestern boundary by the Almonda river. The northwestern part marks the actual end boundary of the Tejo-Sado alluvial aquifer subsystem which would be connected to Tejo-Sado right bank aquifer subsystem. A specified head boundary with the same surface elevation was assigned to examine the interaction between the two aquifer systems.

The two rivers, Tagus and Almonda, were defined as a river package as well as a small stream that cuts through the north part of the study area. Due to the lack of data on the river stage in the national database (SNIRH), the river stage at the stations Barquinha, Chamusca, Ponte Chamusca, and Quinta da Cardiga was used. From the data available at the station Ponte Chamusca, an average depth of 5 meters in the Tagus river was deducted and used in the river package. For the Almonda river as well as the small stream in the north, the DEM was used to assign river stage and an average depth of 1 meter was assumed, based on field observation, and a calculated raster was used to assign for the bottom elevation.

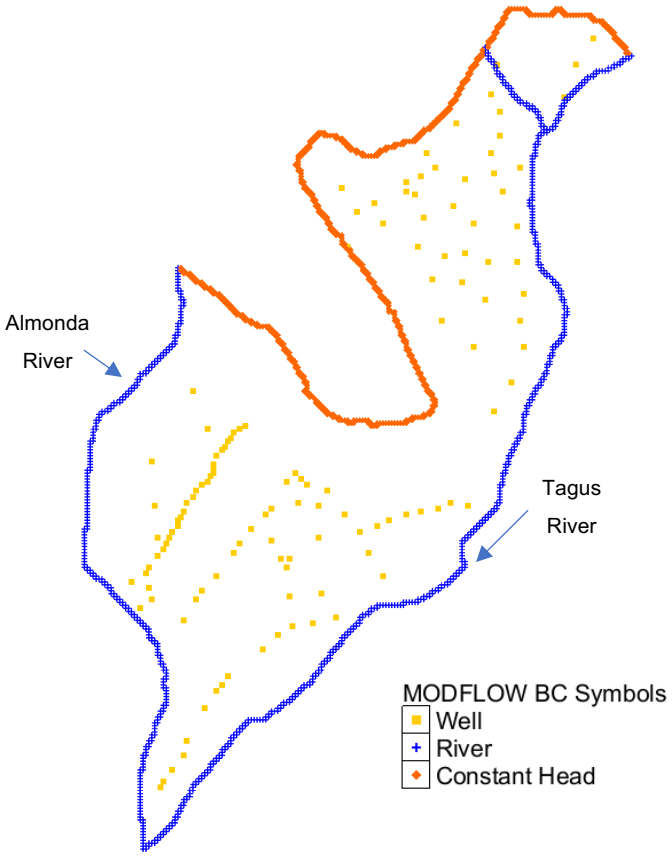

Figure 13: Model Boundary Conditions

The way the river package works in GMS works as follow: by defining river stage and river bottom at specified locations along the river, the elevation and stage are assumed to vary linearly between the points. Thus, the arc defining the river is interpolated linearly between the points. The initial riverbed conductance that was used for the model was calculated using the equation [11]

$$\textbf{Riverbed Leakage} = k \times \mathrm{w} \times \frac{1}{b} \qquad [11]$$

Where k is the riverbed hydraulic conductivity, w is the river width, b is the riverbed thickness over the river segment. The average width of the Tagus river in this area is 250 meters and the thickness of the riverbed material was estimated to be 0.4 meters, thus a riverbed conductance of 40 $m^2/d/m$ was used. And since there is no literature mentioning the Almonda riverbed conductance, the same value was used for the initial model setup as well and then tested for sensitivity.

As for the Paul do Boquilobo wetland, no adequate data could be found to support integrating it into the model, as lake packages in MODFLOW need inputs about lake bed conductance, maximum and minimum stages as so forth. Thus, it was not included in the model as initially planned.

4.3.3 Hydraulic Conductivity

According to the report of the aquifer systems of Portugal, Almeida *et al.*, 2000, the following statistical values of the most important hydraulic characteristics of the Tejo-Sado alluvial aquifer subsystem are provided as shown in Table 1:

Table 1: Aquifer Hydraulic Parameters

Parameter	*Average*	*Median*	*Maximum*
Productivity (l/s)	19.9	12	80
Transmissivity (m^2/d)	1585	1493	5575
Hydraulic Conductivity (m/d)	140	122	464

Where transmissivity is calculated using the formula T=Kh, where T is transmissivity, K is hydraulic conductivity and h is the saturated aquifer thickness. Based on these values, an initial value of 120 m/day was used. Further optimization was done for this parameter and will be discussed in a later section.

4.3.4 Extraction Wells

On July 5th, 2018 a field visit was conducted, and the locations of the pumping wells were noted. It has been noticed that each pivot system has its own pumping well at the center while for other irrigated lands, wells are located along roads where electricity grid is available for energy. This has led to the configuration of the pumping wells as shown in Figure 14. It is noted that there are no pumping wells in the northwestern part of the area, along the Almonda river, as it was verified in the field that all the irrigated lands in this area directly pump water from the Almonda river using surface pumps.

Pumping rates were calculated according to the water needs of the crop type and the area of irrigated land based on the statistical study presented in section 2.4.

By calculating the area of each pivot in the study area and multiplying by the consumption rate, a pumping value was computed for each well inside a pivot. Since there is no way to assign every other well to a specific plot of land, the remaining of the total water need by all the irrigated area was divided by the number of wells outside of the pivots and a constant value was given (1,238 m^3/day). A table with the exact pumping rate of all wells is included in Annex II.

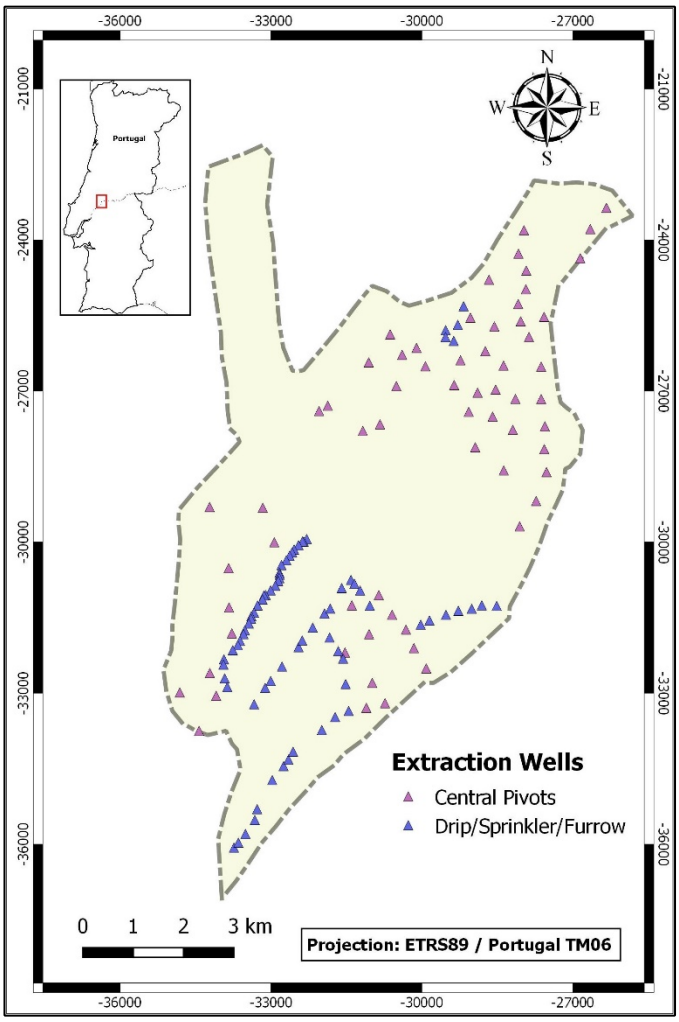

Figure 14: Extraction Wells

4.3.5 Water Budget Zoning

To be able to analyze the individual interaction between each of the Tagus river and Almonda river with the groundwater aquifer system, the study area was divided into three different zones as shown in Figure 15:

- Zone One: Covers the northern part of the study area where the Tagus river bounds from the east, the specified head, representing the interaction with the Tejo-Sado right bank aquifer subsystem, bounds from the west and a small stream that flows into the Tagus. Also, 60 % of the pivot extraction wells are in this zone.
- Zone Two: Covers the south-east part of the study area where the Tagus river bounds from the west and the less dense area of the extraction wells in the south are.
- Zone Three: Covers the southeastern part of the study area where the Almonda river bounds from the west and the specified head bounds from the north. The highly dense extraction wells are in this zone.

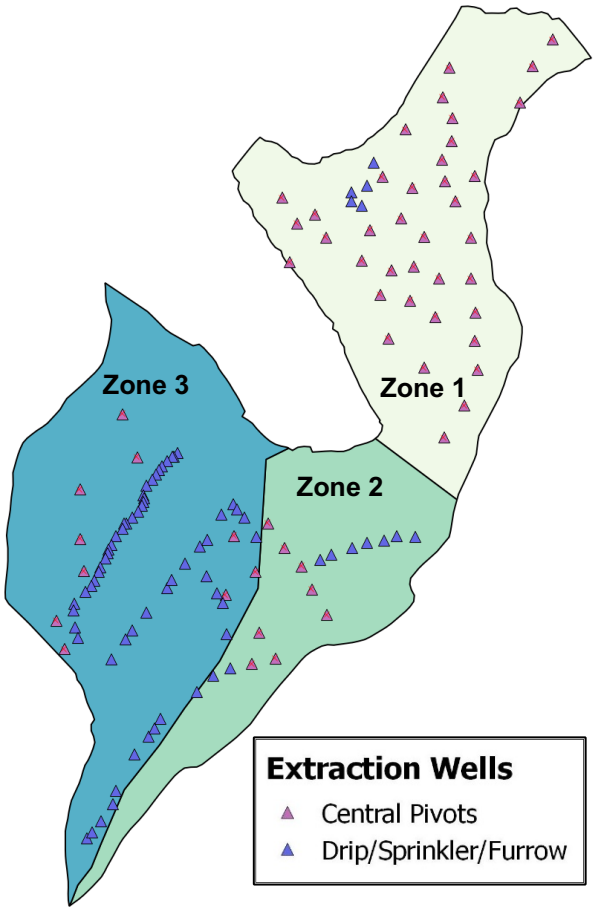

Figure 15: Water budget zones

4.3.6 Model Calibration

Model calibration is an essential part of the groundwater flow modeling process. For a model to be used for predictions of future scenarios, it must be demonstrated that it can fit the observed aquifer behavior. Calibration is the process of systematically altering certain model parameters and the model is repeatedly run until the computed solution matches the observed values within an acceptable confidence level.

During the field visit, 4 wells were found accessible to measure water level in them. These wells along with one piezometer available in the national monitoring network (SNIRH) were used as calibration points for the model.

The final step towards calibration is performing a sensitivity analysis to test the sensitivity of the water budget of the study area, represented in the rivers-aquifer interaction, towards the hydraulic parameters and the pumping rates. Aquifer hydraulic conductivity and river conductance where systematically changed in the model input packages and the results were noted. To quantify the model sensitivity and performance several indicators were used. First, the sum of squared differences between the observed and modeled head values at the observation points was calculated and correlated to the initial run.

The Nash Sutcliffe coefficient, NSE, by Nash and Sutcliffe, 1970 was used to measure the model efficiency and performance. The NSE is a way to measure the fit between predicted and measured values. It measures the sum of deviations of the observations of the observations from a linear regression line with a slope of one. If the observed values are equal to the predicted values, a NSE value of one is obtained. The equation to calculate the NSE is as follows:

$$\mathbf{NSE} = \frac{\sum_{i-1}^{n}(\boldsymbol{Q_m} - \overline{\boldsymbol{Q_m}})^2 - \sum_{i-1}^{n}(\boldsymbol{Q_m} - \boldsymbol{Q_p})^2}{\sum_{i-1}^{n}(\boldsymbol{Q_m} - \overline{\boldsymbol{Q_m}})^2} \qquad [12]$$

Where; Q_m is the measure value, Q_p is the predicted value and the $\overline{Q_m}$ is the arithmetic mean of the measured value.

Using an automatic parameter estimation method (PEST) on GMS software, the spatial distribution of the hydraulic conductivity was estimated aiming for a better fit model. PEST is an inverse modeling technique that iteratively adjusts a one or several parameters and repeatedly launches the model until the computed output is equal to the observed values or until the error is minimized. A pilot point guided inverse model estimates the parameter at the pilot points to minimize the objective function. A 2D scatter point grid was created with a spacing of 500 meters in the x and y directions to guide the automatic estimation inverse model. A total number of 213 pilot points were used as shown in Figure 16. The optimal value of hydraulic conductivity obtained from manual calibration was given as an initial value for guiding the inverse model at the pilot points. The PEST then starts altering the parameter within the range of values predefined until an optimal solution is reached. In the case of no convergence at any of the pilot points, the initial value defined is given to the pilot point.

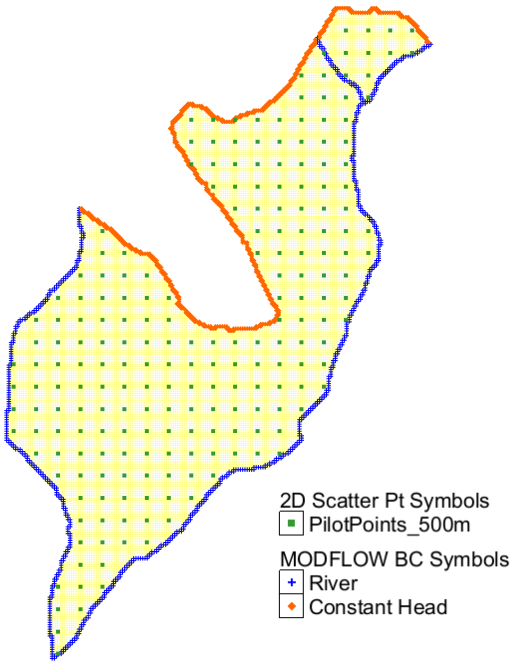

Figure 16: Pilot points

5 Results & Discussion

In this section, the results of all the modeling scenarios as well as the recharge calculation process are presented and discussed in detail.

5.1 Recharge Estimation

The first objective of this research is to estimate the recharge rate as well as the total recharge volume of the shallow Tejo-Sado alluvial aquifer in the proximity of the city of Golegã. The SPEI index was chosen to identify a normal year, where the SPEI value is lowest, to be used as the modeled period. Results obtained are shown in Figure 17 for the past 27 years. A hydrological or water year starts in October, in the northern hemisphere, and ends in September of the next year. In October, the hydrological cycle is at balance and afterward, the rainfall starts to fill up the water reserves until April when evaporation starts the depletion process from the reserves until end of September and then the cycle starts again in October (Water UK, 2012). The hydrologic year of 2015/2016 shows the lowest overall SPEI values since 2010 and thus was chosen for the modeling period.

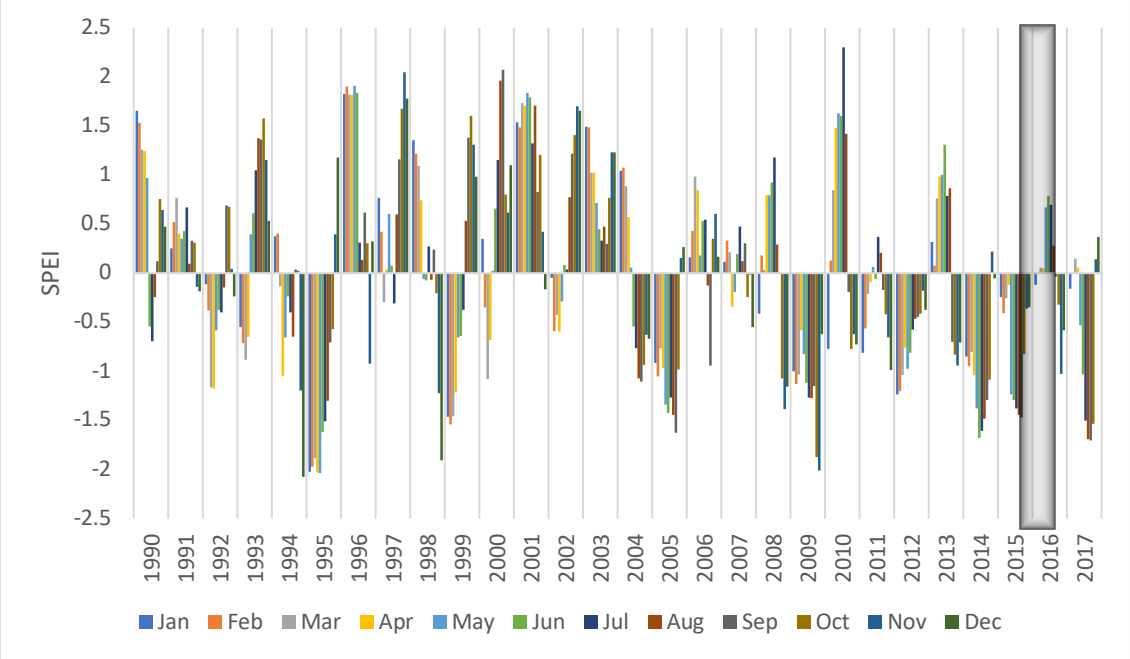

Figure 17: SPEI Drought Index

Next, evapotranspiration was calculated using available climate data as discussed in earlier sections and the results are shown in Figure 18, where potential evapotranspiration calculated using the Penman-Monteith method along with the actual evapotranspiration calculated using the MODIS layers are plotted. By comparing both, it is noted that the real evapotranspiration is always lower than the potential evapotranspiration, which gives the data a high confidence level except for only one month, December 2015.

The difference between precipitation and real evapotranspiration, Pt-ETR, is also shown to define the periods when water deficit exists, which indicates more pressure on the groundwater resource. This shows a great deficit in the months of June to September, which coincides with the peak demand by maize during July. The graph shows water surplus in the months of October to February as well as April and May. This surplus indicates groundwater recharge periods. The water balance indicates a total surplus of 344 mm as a potential recharge to the groundwater from precipitation in the whole year. With a total annual precipitation of 573 mm, recharge represents 60% of the total annual precipitation in the study area. This percentage is considered very high in comparison to literature that suggests a recharge percentage of 30% of the total annual precipitation (A.P.A., 2012 & Almeida *et al.*, 2000). This very high value is due to the simple calculation used in this method where only precipitation and evapotranspiration are considered in the water balance equation. In more complex methods, the storage capacity of the aquifer and the thickness of the vadose zone plays an important role in the water balance.

By subtracting the calculated real evapotranspiration from the mean monthly precipitation, the spatial and temporal distribution of the recharge of the study area as shown in Figure 19. Temporally, October, January, and May show significantly high recharge rates in relation to the other months with this hydrological year but generally recharge periods are defined between October and may, while summer months, July to September, show the lowest values of recharge. There is no specific spatial trend noticed in the monthly data sets. White or empty grids within the datasets are no data points that is due to the cloud cover that doesn't enable satellite measurements from being processed.

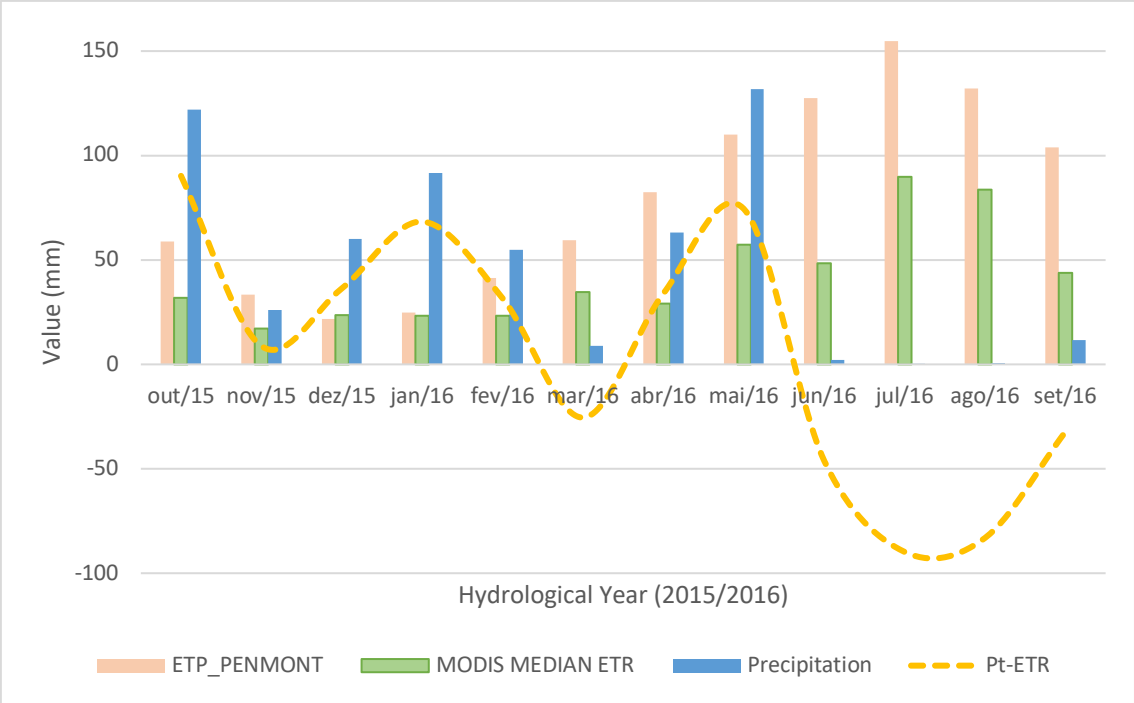

Figure 18: Water Balance

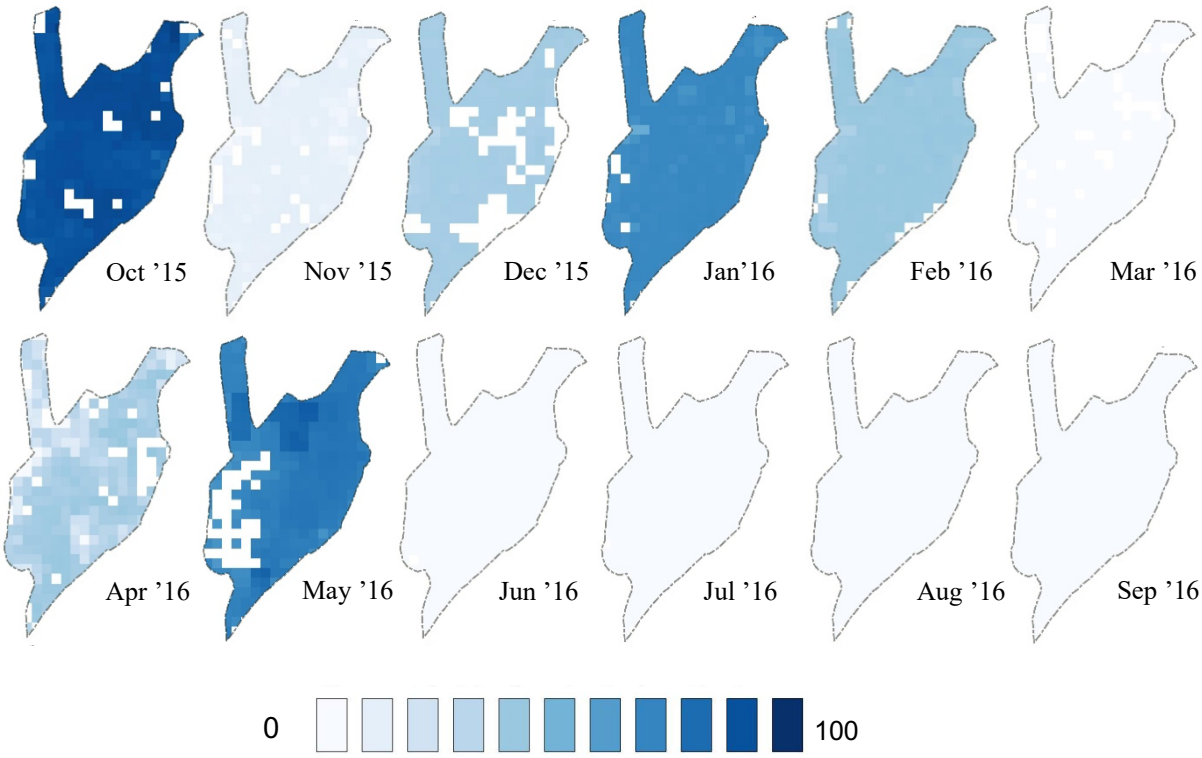

Figure 19: Spatial & temporal distribution of total monthly recharge in mm

After processing the 12 raster maps, they were summed up to give the spatial distribution of the total annual real evapotranspiration, shown in Figure 20. The resulting raster has the same resolution of the original MODIS layers, 500 m resolution. The map shows a wide range of recharge values from a maximum of 0.00082 m/day and a median of 0.0007 m/day. There is no specific spatial trend or focal points in terms of recharge noticed from the results, yet, a high recharge area exists in the central part of the study area, south west of the city of Golegã. Another high recharge area is in the northern high relief area which does not make sense in terms of water flow as the water is expected to run on the surface towards the eastern lowlands into the river.

Relatively low recharge is noticed in the southwestern part of the study area where the Paul do Boquilobo biosphere reserve exists. This is due to the high evapotranspiration rates in this area because of the dense vegetation in the reserve area as well as the evaporation from the wetland within.

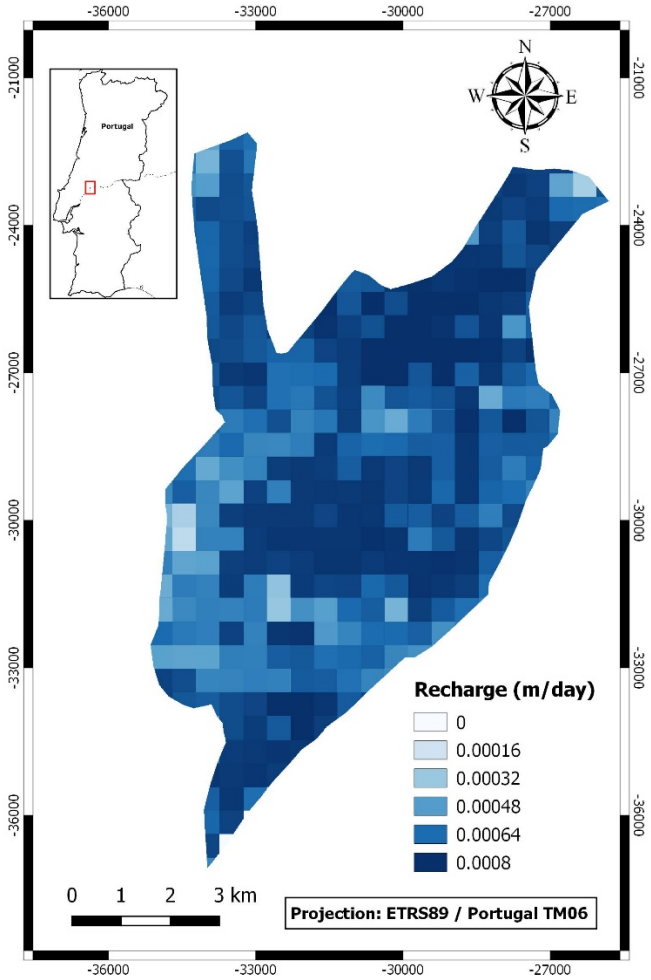

Figure 20: Total annual recharge (m/day)

5.2 Pre-calibrated Flow Model

Results of the numerical groundwater flow model can be previewed and analyzed in two different aspects; quantitatively in terms of water budget and flow volumes of the interactions between the different water bodies and qualitatively in terms of groundwater flow direction trends within the study area.

The total volumetric in/outflow balance is 901,018 m^3 with a percentage of discrepancy between In and outflow volumes of 9×10^{-6}. This is the first indication of the good performance of the model. To further check the model performance, the sum of squared difference of the observation wells is calculated and it is 5.176 m^2, which is minimal and indicates good model performance as well. The last model performance indicator used is the Nash–Sutcliffe model efficiency coefficient (NSE), which was 0.91. The closer NSE value to one, the better the model performance is. Thus, the overall performance of the model so far is good. It must be noted that only five observation points exist in the study area and mainly concentrated in the southern part of the study area, 4 of which show very good prediction error with a maximum difference of 0.87 meters from observed values, shown in Figure 21. The fifth observation point shows 1.84 meters of difference in head

between observed and simulated values and this is due to its location very close to the specified head boundary that maintains the head constantly high in the proximity.

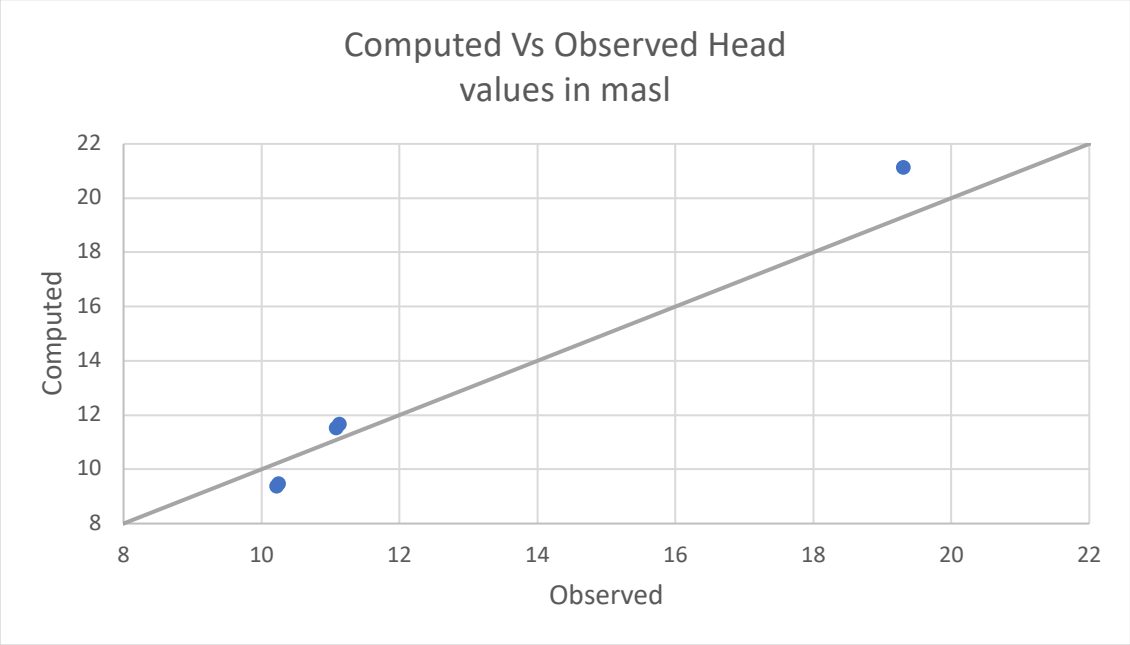

Figure 21: Observation Wells Residuals

Water Budget

Figure 22 shows the global water budget of the initial groundwater flow model. Results indicate that the constant head and river leakage have the highest contribution to the water budget. On the inflow side of the budget, the constant head has the highest contribution with 84% of the total inflow volume into the aquifer system while river leakage and recharge contribute by 12% and 4% respectively. In absolute values, the constant head boundary inflows 756,098 m^3/day while all rivers inflow 109,831 m^3/day into the aquifer system. On the outflow side of the budget, constant and river leakage contribution are very close to each other with 46% and 42% of the outflow is contributed respectively, while extraction wells for agriculture use consume 12% of the total outflow with a total extraction rate of 109,290 m^3/day. Total outflow from the aquifer system to the contact head boundary is 411,553 m^3/day and 380,175 m^3/day outflows towards the rivers.

To analyze the individual interactions between each river and the aquifer system, the zonal water budget is examined. Figure 23 shows the percentage of inflow and outflow for each boundary in relation to the total inflows and outflows. 92% of the inflow from the constant head boundary flows into zone one, the northern part of the study area. This boundary marks the highest topographic relief in the area and since groundwater flow follows the surface gradient, the flow is coming from the constant head boundary in the west to the east towards the Tagus river. This flow represents the contribution from the neighboring groundwater aquifer, Tejo-Sado right bank aquifer subsystem. As for the river leakage, 90% of the inflow from rivers into the aquifer system is through zone 3, which has the Almonda river at its western boundary. This leads to a contribution of 98,560 m^3/day from the Almonda river into the aquifer. This is followed by 9% of river

contribution in zone one, which represents the flow from the small stream in the north part of the study area that flows eventually into the Tagus river.

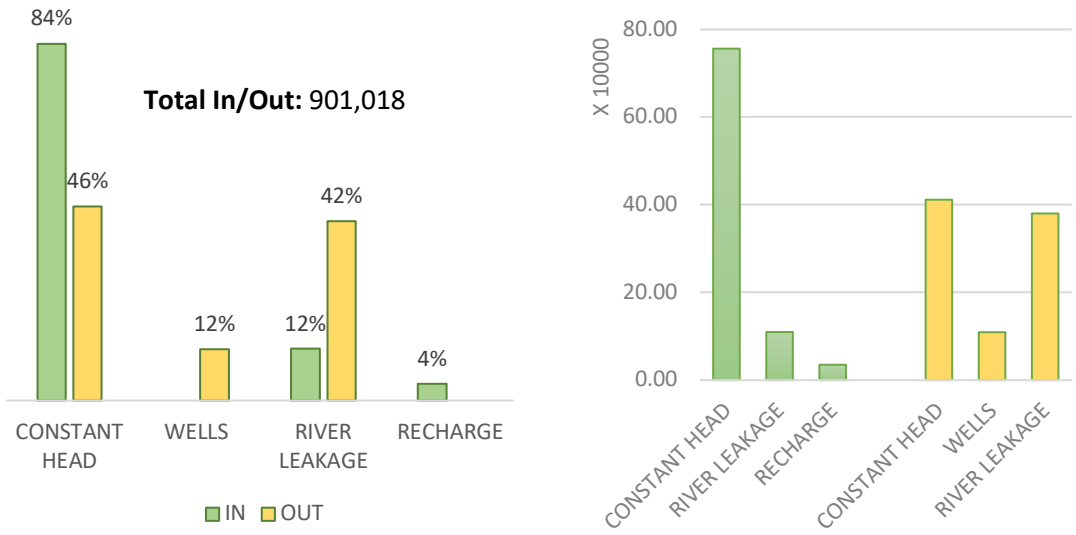

Figure 22: Global Water Budget of Initial Model (Left: Percentage from the total in/out, Right: Total flow in m3/day)

In the outflows, 93% of the total outflow towards the constant head boundary is in zone one, which can be better explained when looking at groundwater flow contours in the next sections. In terms of river leakage outflows, 81% flows out in zone one where the Tagus river is the main boundary in the east along with the small stream flowing towards it as well. Yet another 5% flows out towards the Tagus river represented in zone two and lastly, 14% of the total aquifer outflows to rivers discharge in the Almonda river, indicated in zone three.

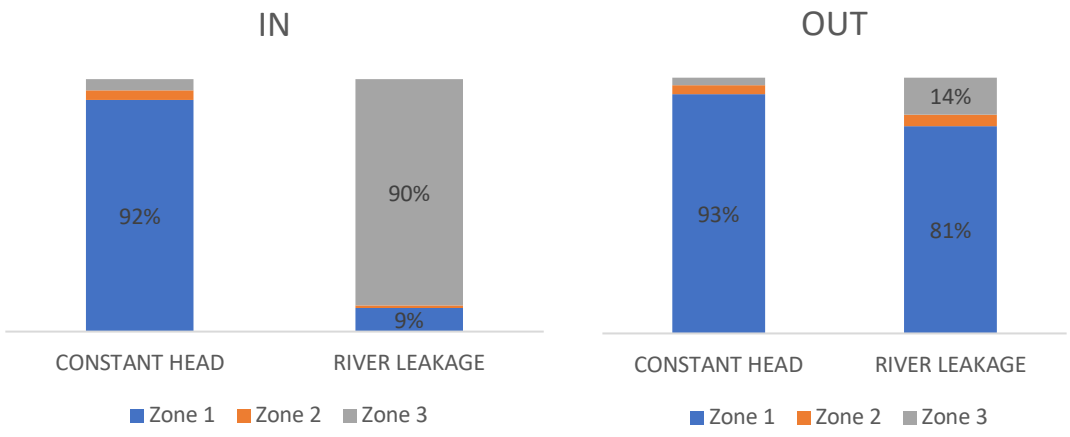

Figure 23: Zonal Water Budget (Initial Model)

By calculating the difference between the total inflow and total outflow of zones one and two together, the relationship between the aquifer system and the Tagus river can be analyzed. After subtracting the total outflow from the total inflow from river leakage a deficit of 314,301 m^3/day was found. Knowing that the Tagus boundary on the east is 17 km long, this gives a discharge of

18,488 m^3/day/km into the river. This concludes that the aquifer contributes to the Tagus river discharge especially in the northern part, zone one, where the high gradient induces the flow towards the river and a widely distributed extraction wells distribution does not put too much pressure on the groundwater resource as it is compensated from the constant head boundary. As for the Almonda river, a surplus of 43,957 m^3/day is calculated, meaning that the river contributes to the aquifer much more than the aquifer contribution to the river discharge. Almonda river boundary is 11 km long, which concludes a total discharge of 3,996 m^3/day/km into the aquifer.

Groundwater Flow Direction

According to the groundwater flow direction, three flow patterns can be deducted as shown in Figure 24. The first is the flow of the groundwater from west to east in the northern part of the study area following the surface topography and indicates groundwater interaction between the western constant head boundary and the aquifer and the inflow towards the Tagus river in the east boundary.

The second groundwater flow pattern is in the southwest part of the study area, where groundwater is flowing to the south/southeast from the constant head boundary and the Almonda river as well towards the aquifer. This groundwater flow pattern is induced and intensified by the extraction wells in this zone where the density of the wells is the highest in the study area.

The third pattern noted is the flow from the Tagus river in the east towards the aquifer feeding the groundwater extraction wells for agriculture.

5.3 Model Calibration

5.3.1 Sensitivity Analysis

The first step into model calibration was performing a sensitivity analysis to define the hydrological parameters which the model is sensitive to. A systematic trial and error method was used and resulted in the following results presented in Table 2. Change in SSD is the difference between the initial model SSD and the sensitivity simulation SSD. The change % is the ratio between the change in SSD and the initial SSD.

At a constant hydraulic conductivity, like initial model conditions, river bed conductance was changed in the following manner: the multipliers 0.5, 2 and 4 were tested sequentially and 2 different indicators were used to test sensitivity as described in section 4.3.6. The first multiplier resulted in a decrease of SSD by 5% while the second and the third resulted in improvements of 3% and 5% respectively. Since the improvement from the second to the third multiplier resulted in only 2% of improvement, and a total 5% from the initial SSD, the model was considered not significantly sensitive to riverbed conductance and the value of 160 m/day was set to be the best estimation.

Then at the initial river conductance value, 40 m/day, the hydraulic conductivity of the aquifer was systematically altered, and indicators were noted. The first multiplier, 0.5, resulted in the most

significant decrease in the SSD with 1053% decrease in performance compared to the initial model and giving the worse NSE value obtained through the process, 0.013. This was already giving an indication of significant sensitivity towards the hydraulic conductivity of the aquifer. The second multipliers; 2, still resulted in a decrease in the model performance by 64% and thus a decreasing the multipliers again by half the interval was adopted to reach better fit in the model outcome. The multipliers 1.5 and 1.25 were used and resulted in a decrease of 8% and an increase of 12%% respectively. The last trial was at a hydraulic conductivity of 150 m/day and that was further used as the optimal solution for manual calibration.

Table 2: Qualitative sensitivity analysis indicators (RC: Riverbed Conductance, HK: Hydraulic Conductivity)

PARAMETER	RC (M/DAY)	HK (M/DAY)	MULTIPLIER	SSD	CHANGE IN SSD	CHANGE %	NSE
INITIAL CONDITIONS	40	120		5.176			0.914
RC 1	20	120	0.5	5.454	-0.278	-5%	0.910
RC 2	80	120	2	5.028	0.148	3%	0.917
RC 3	160	120	4	4.930	0.246	5%	0.918
HK 1	40	60	0.5	59.665	-54.488	-1053%	0.013
HK 2	40	240	2	8.466	-3.290	-64%	0.860
HK 3	40	180	1.5	5.581	-0.404	-8%	0.908
HK 4	40	150	1.25	4.539	0.636	12%	0.925

Further on, one simulation was run with zero recharge input to test the model performance and sensitivity toward recharge and this resulted in a 48% decrease in the SSD which indicates sensitivity to recharge and indicates good recharge estimation. Overall, using the qualitative indicators of model performance, it was proved that the model is significantly sensitive towards the hydraulic conductivity and less or even slightly sensitive towards riverbed conductance.

To quantitatively assess the model, absolute water budget components were tested during the sensitivity analysis process. Changing the river bed conductance showed significant changes in river leakage in both Inflow and outflow with a maximum change of 110% and 48% of the initial model respectively. While constant head contributions had minimal changes of a maximum of 6%. This was the expected result as changing the river bed conductance directly affects the flow from and to the river boundaries. As for testing sensitivity of the aquifer hydraulic conductivity, significant changes in flow values from and into the constant head boundary is noticed with the highest change of 91% in the inflow and 107% in the outflow both at twice the initial hydraulic conductivity value.

Conclusively, the optimal values for the two variables after sensitivity analysis and manual calibration were 160 m/day hydraulic conductivity and 150 m/day riverbed conductance. These values have resulted in a 15% improvement in the model performance in the SSD and 2% in the NSE.

5.3.2 Automatic Parameter Estimation (PEST)

The second step in model calibration is using an automatic parameter estimation method called PEST that is embedded in the GMS software and can be applied to MODFLOW as an inverse modeling technique. As described earlier in section 4.3.6, 213 pilot points were used with a spacing of 500 m in both x and y directions as in Figure 16. The main reason behind this method is not only to try to better fit the model but also to estimate the special distribution of the hydraulic conductivity of the aquifer to better understand the hydrodynamics of the aquifer system.

An initial value of 150 m/day of hydraulic conductivity was given to the points to guide the inverse model iteration process. A minimum of 80 m/day and a maximum of 200 m/day were used as the limiting values of hydraulic conductivity as described in the previous literature (section 4.3.3).

Figure 24 shows the computed groundwater flow heads overlain by arrows of the vector direction of the groundwater flow. The scale of the flow vectors is proportional to the magnitude, thus longer arrows indicate higher flow velocity. In relation to the initial model, both plotted in Figure 24, there is no significant change in the magnitude of the groundwater flow. By comparing the groundwater flow direction, a minor change in the flow direction is noticed at the west with the constant head boundary, which will affect the absolute water budget values, but the general direction is maintained flowing from the west to the east and flowing into the Tagus river. In the southern part, a change in the computed head is noticed especially closer to the Tagus river. The drawdown is reduced by around one meter, contour ten indicates the change and the direction of the flow close to the river reversed from going towards the river to be more parallel to or towards the Tagus river.

To test the model performance and calibration validity, the SSD and NSE were computed and compared to the initial model setup before calibration. This model resulted in a SSD of 3.09, 60% improvement, and a NSE of 0.96, 6% improvement. In terms of the global water budget, Figure 25, the total volume of inflows and outflows has increased by 9.5% to a value of 986,313 m^3/day. The constant head boundary contributes by almost 70% of the inflow to the system while river and the recharge contribute by 28% and 4% respectively. In the outflows, the aquifer is losing more water to the river by almost 60% of the total outflow while 31% is outflowing to the constant head boundary mainly in the northern part, zone one.

To emphasize the effect of the extraction wells and analyze the response of the groundwater head and water table toward the extraction for agricultural lands in the study area, a simulation was run using the output hydraulic conductivity from the PEST simulation and with zero extractions. By subtracting the computed head of the simulation with extraction from the computed head with no extraction, a drawdown map was produced as shown in Figure 26. Significant drawdown, up to 3.5 meters, is shown because of the groundwater extraction. The northern part of the study area has only 0.4 meters of drawdown for two reasons, compensation of extracted water from the western boundary of the constant head which is representing the inflow from the

neighboring Tejo-Sado right bank aquifer subsystem and the other reason is the relatively low density of distribution of the wells in comparison to the southern art.

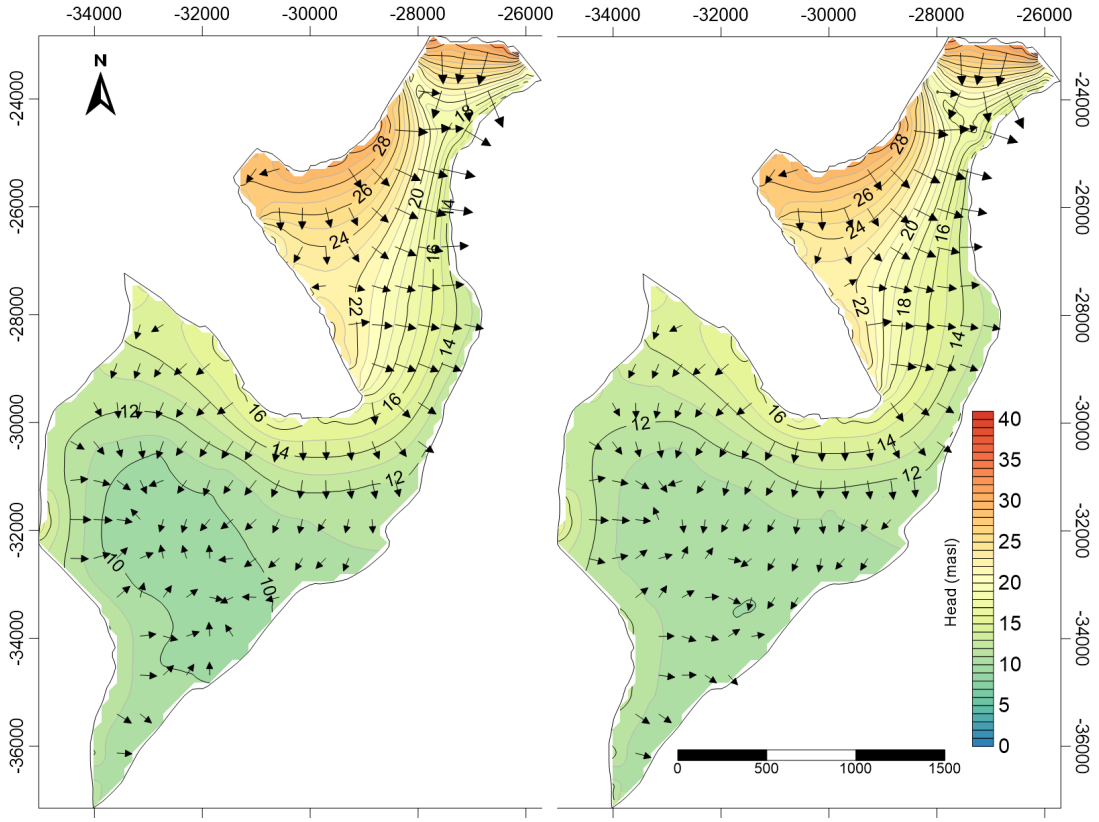

Figure 24: Groundwater Flow in the Pre-Calibrated Model (Left) and the PEST Calibrated Model (Right)

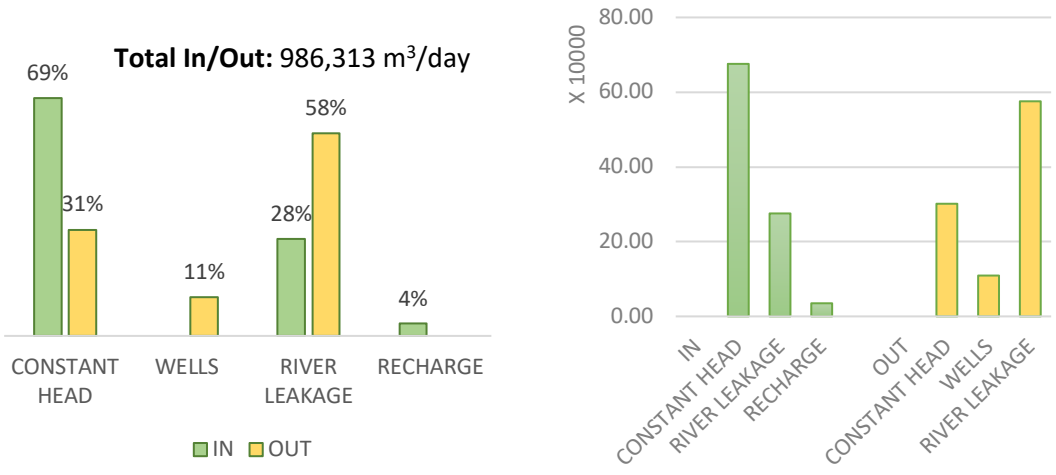

Figure 25: Global Water Budget of PEST calibrated Model (Left: Percentage from the total in/out, Right: Total flow in m3/day

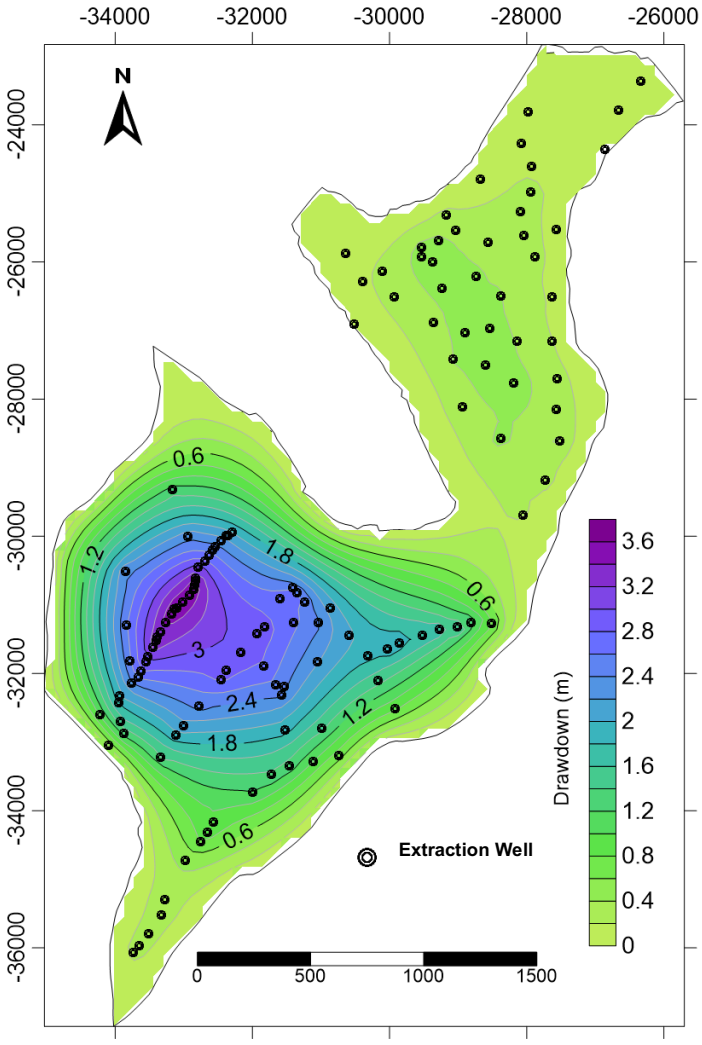

Figure 26: Drawdown in PEST calibrated model

The drawdown is focused and concentrated around the highly dense area with extraction wells. This density is a result of the limitation in the distribution of the electric utility in that area that forces people to build their wells along the grid distribution network lines. The result shows that these extraction wells are inducing the main groundwater flow direction in the south and consuming water infiltrating from the Almonda river from the west, the contribution from the Tejo-Sado right bank aquifer subsystem from the north and from the Tagus in the east.

Finally, the analysis of the computed hydraulic conductivity from the automatic parameter estimation method was made and correlated to observed aquifer properties. Figure 27 shows the spatial distribution map of the computed aquifer hydraulic conductivity. The map shows an increasing trend in the hydraulic conductivity from west to east. Zone one shows a very significant high gradient in hydraulic conductivity. In the south, zones two and three, show a gentle gradient from north to south increasing toward the riverside.

Two reasons can explain this trend. First, is that according to Darcy's law, the specific discharge is directly proportional to the hydraulic gradient. Since the northwestern part of the study area is the highest topographic region, and groundwater flow is assumed to follow the surface gradient,

then specific discharge will increase in the same manner and hence the hydraulic conductivity. The second reason can be deduced by looking at the aquifer thickness map in Figure 27. The change in the aquifer thickness, in the north, from 80 meters thick to 20 meters in 2.5 to 3 km span, increases the groundwater flow velocity as it is pushed into a smaller cross-section.

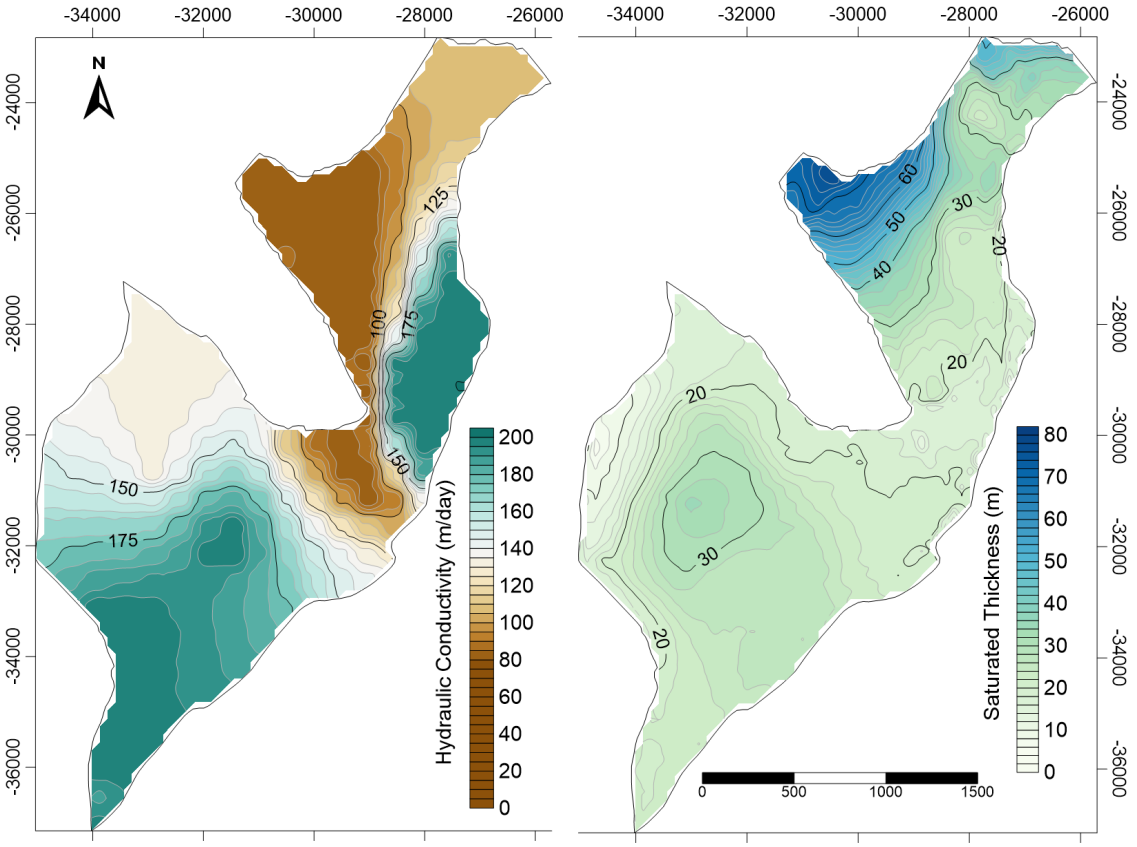

Figure 27: Estimated Hydraulic Conductivity (Left) and Aquifer Thickness (Right)

Considering h as the fully saturated part of the aquifer, bounded between the bottom and the water table level which is considered as the surface level in this study as the initial head, the transmissivity, T, of the aquifer follows the law T=Kh, and thus hydraulic conductivity is inversely proportional to the saturated thickness of the aquifer. And since the thickness decreases in the northern part from west to east, the hydraulic conductivity should be increasing accordingly.

In the southern part, especially zone three, the effect of the aquifer thickness if emphasized in the central part but not as much as it shows in the northern part as the effect of dense pumping along with the inflow from the river induce groundwater movement and flow velocity is increased leading to an increase in calculated hydraulic conductivity according to Darcy's law.

5.4 Climate Change & Adaptation Scenarios

In the pursuit of improving the water resource management of the study area and incorporation adaptation measures climate change and/or climate variability conditions in the area, two scenarios were simulated for future conditions to assess the effect of groundwater flow patterns

and sustainability of the resource under future conditions. The PEST calibrated Model is used as the reference scenario in this section.

5.4.1 Recharge Decrease

The report of climate change scenarios of Portugal by Miranda *et al.*, 2002, shows the relative change in accumulated precipitation under climate warming scenario, HadRM GGa2 simulation. The results in Figure 28, show an overall decrease in the total annual precipitation in most of Portugal, especially in the Alentejo region. Nevertheless, the seasonal distribution of this change in precipitation amount is not equally divided. It shows that during winter, total accumulated precipitation can increase by up to 150%, while all other seasons show a decrease in the precipitation. Spring precipitation can decrease by up to 10%, autumn shows a decrease of up to 60% and summer precipitation decreases by up to 85%. Although summer shows the maximum percentage of decrease in accumulated precipitation, the amount of rainfall during summer is significantly low that makes the decrease during spring and autumn times much more significant in terms of the effect on total annual precipitation.

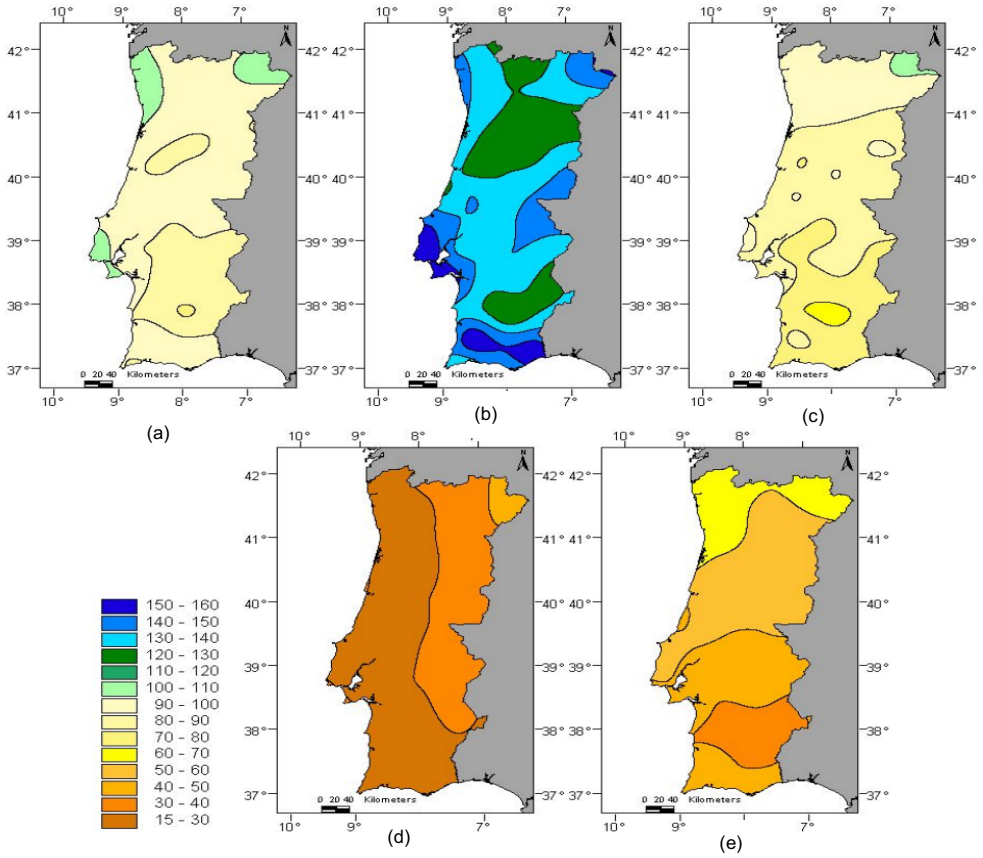

Figure 28: Annual and seasonal total precipitation in HadRM GGa2 simulation (% from control). (a) annual; (b) winter; (c)Spring; (d) Summer; (e) Autumn

Table 3 shows the actual seasonal precipitation values of the hydrological year of 2015/2016 along with the estimated seasonal precipitation values for the future climate change scenario. An increase of 50% in precipitation during winter and a decrease of 10%, 85% and 60% during spring,

summer, and autumn respectively. The total annual precipitation decreases from 573 mm to 558 mm by a percentage of 3%.

Table 3: Current & future seasonal precipitation

	Decrease	Increase
Winter		50%
Spring	10%	
Summer	85%	
Autumn	60%	

			Current	Future
PPT in climate change HadRM GGa2 Simulation (mm)	Autumn	October	122	48.8
		November	26	10.4
	Winter	December	60	90
		January	91.6	137.4
		February	54.8	82.2
	Spring	March	9	8.1
		April	63.2	56.88
		May	131.8	118.62
	Summer	June	2.2	0.33
		July	0.1	0.015
		August	0.6	0.09
	Autumn	September	11.6	4.64
Total			572.9	557.475
				97%

As for temperature change in the same climate change scenario, Table 4 shows the anomalies of change at the maximum and minimum temperature in the region of the study area as derived from Miranda *et al.*, 2002. The maximum increase in average temperature is 8°C during summer time and the minimum increase is 4°C during winter time. It is also worth to mention that the anomaly of the maximum temperature during winter is smaller than that of the minimum temperature during the same season.

Using the Thornthwaite method of calculating potential evapotranspiration, which depends on the monthly temperature and the sunshine hours of the latitude of the area, the future potential evapotranspiration was calculated, and results are shown in Table 4. Results show very high evapotranspiration values in comparison to the current real evapotranspiration values obtained before using MODIS dataset. This is expected due to the significant increase in average monthly temperature, especially during the summer season when the maize is at its peak flourish. Finally, subtracting potential evapotranspiration from precipitation is calculated to estimate groundwater recharge for the future scenario. A total annual recharge of 136 mm is estimated. This recharge takes place only during the winter months, December, January, and February, with a monthly recharge of 36, 80 and 20 mm respectively. This is due to the significant increase in precipitation during these months, coinciding with the months of the lowest evapotranspiration as well.

Table 4: Temperature anomalies and Monthly PET in Climate Change scenario

Temperature °C		Current		Anomaly (+ve)		Future			Future PET (mm)
		Min	Max	Min	Max	Min	Max	Avg	
Autumn	October	15.2	22.1	6	7.5	21.2	29.6	25.4	111
	November	10.4	18.6	6	7.5	16.4	26.1	21.25	79
Winter	December	7	15.6	5.5	4	12.5	19.6	16.05	54
	January	7.7	16.4	5.5	4	13.2	20.4	16.8	58
	February	7.1	16	5.5	4	12.6	20	16.3	62
Spring	March	9.7	14.6	5	5.5	14.7	20.1	17.4	75
	April	10.4	17.6	5	5.5	15.4	23.1	19.25	92
	May	13.7	21.8	5	5.5	18.7	27.3	23	124
Summer	June	17.6	24.9	6.5	8	24.1	32.9	28.5	176
	July	19	26.7	6.5	8	25.5	34.7	30.1	189
	August	20.1	26.9	6.5	8	26.6	34.9	30.75	183
Autumn	September	17.5	26.9	6	7.5	23.5	34.4	28.95	151

With a total annual precipitation of 558 mm and a total annual recharge of 136 mm, groundwater recharge represents 24% of the total the annual precipitation. In comparison to the ratio calculated in section 5.1, where recharge represented 60% of the total annual precipitation, a significant reduction in precipitation contribution to groundwater recharge is noticed due to climate warming scenario in the future. Thus, to be able to import the new recharge value to the groundwater flow model, the units must be presented in m/day. This concludes with a daily recharge of 0.00037 m/day.

A constant recharge value is given to all MODFLOW cells in the groundwater flow model. This simplification to the model is due to the unpredictability of the spatial distribution of the potential evapotranspiration in the study area in a time interval of 80 years. The results of the groundwater flow model are presented in Figure 29. Groundwater heads don't show a significant change from the reference scenario throughout the study area, except at the southern part where extraction wells exist that induce local drawdown areas. One of these local areas is close to the Tagus river, which divers the groundwater flow direction toward the extractions wells increasing the flow from the river to the aquifer system.

By calculating the difference in head between the reference scenario and this scenario, the plot on the right in Figure 29 is produced, where the head of the reference scenario is subtracted from this scenario's head result. The result shows a negative difference indicating an increase in the drawdown due to the decrease in total recharge from precipitation. The maximum decrease in drawdown noticed is 0.22 m, which is considered non-significant with respect to the scale of extraction in the study area. This small increase in drawdown is probably due to the compensation from the inflow of groundwater from the western boundaries, the constant head, and the Almonda river. Due to the steady state conditions of the model, the decrease in recharge would induce more water to inflow from the boundaries, especially the constant head boundary, to compensate and stabilize the groundwater flow budget. Thus, the water budget was analyzed to test the validity of this hypothesis.

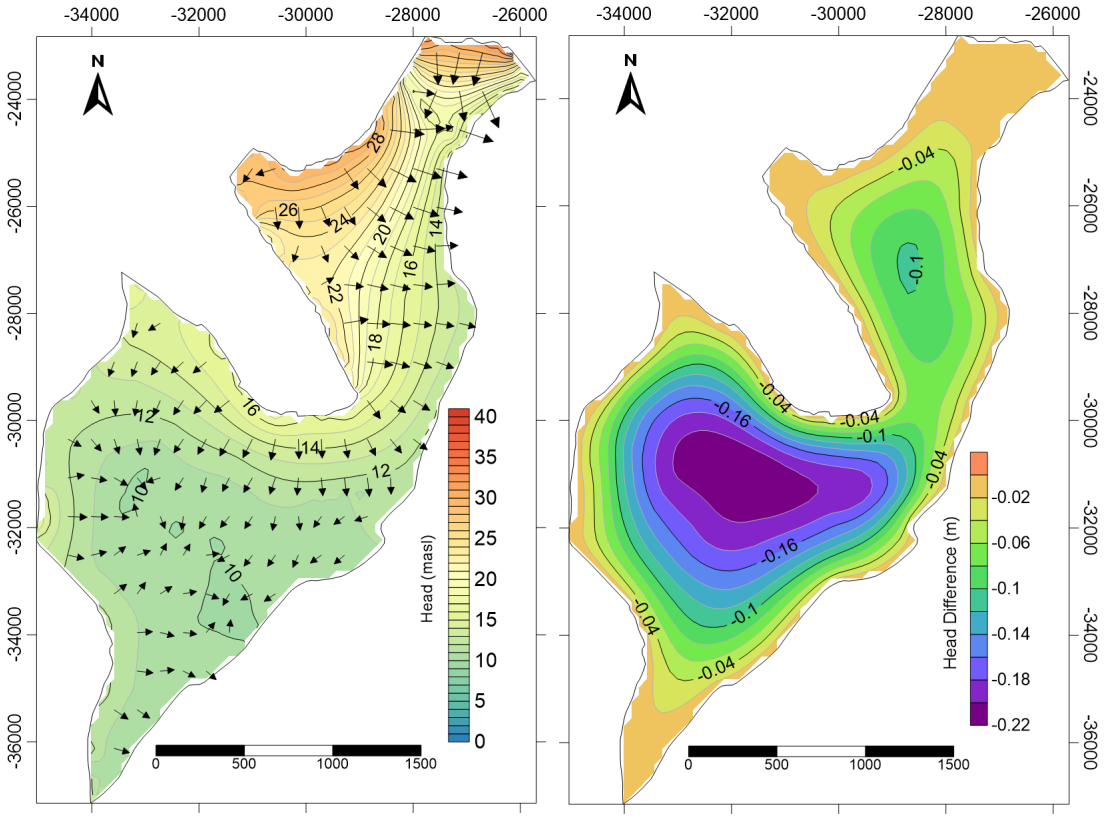

Figure 29: Groundwater head and flow direction (Left) and Difference in head from reference scenario (Right)

Table 6 show the flow rates into and out of the aquifer system from each of the rivers and indicates that the Almonda river in both scenarios has higher inflow than outflow from the aquifer, which means that Almonda river is contributing to the aquifer as expected from the flow direction map. The difference in the net flows between the two scenarios shows an increase in the inflow from the Almonda river under climate change scenario by 3,026 m^3/day and a total volume of 1.1 hm^3 flows into the aquifer in this scenario than the reference scenario. The decrease in recharge was partially compensated by more inflow from the river towards the extraction wells. In percentage, the net difference between the scenarios shows a 5% increase in river contribution under climate change scenario.

The constant head boundary also contributes to compensate the decrease of recharge over the study area. The results in Table 5 show an increase in the inflow towards the aquifer from the constant head boundary with a total volume increase of 2.1 hm^3/day, which is a 2% increase from the reference scenario contribution. Although zone one holds the highest gradient of flow and the highest contribution from the constant head boundary is expected in this zone, 40% of the increase in the inflow is in zones two & three and this is due to the high density of extraction wells that induces groundwater flow towards them.

Table 5: Constant Head water budget Comparison; (A) Total, (B) Zones two + three

	ALMONDA (IN) (M^3/DAY)	ALMONDA (OUT) (M^3/DAY)	IN-OUT (M^3/DAY)
REFERENCE SCENARIO	240,995	176,449	64,546
CLIMATE CHANGE SCENARIO	242,498	174,926	67,572
(A)	**(Reference - CC Scenario) in m^3/day**		-3,026
	Difference in m^3/year		-1,104,373

	TAGUS (IN) (M^3/DAY)	TAGUS (OUT) (M^3/DAY)	IN-OUT (M^3/DAY)
REFERENCE SCENARIO	34,503	399,136	-364,632
CLIMATE CHANGE SCENARIO	35,084	392,788	-357,704
(B)	**(Reference - CC Scenario) in m^3/day**		-6,928
	Difference in m^3/year		-2,528,780

Table 6: Almonda water budget (A) and Tagus water budget (B)

TOTAL CONSTANT HEAD BALANCE	CONSTANT (IN) (M^3/DAY)	CONSTANT (OUT) (M^3/DAY)	IN-OUT (M^3/DAY)
REFERENCE SCENARIO	675,726	301,439	374,286
CLIMATE CHANGE	679,874	299,808	380,066
(A)	**(Reference - CC Scenario) in m^3/day**		-5,780
	Difference in m^3/year		-2,109,548

CONSTANT HEAD IN ZONES 2 & 3	CONSTANT (IN) (M^3/DAY)	CONSTANT (OUT) (M^3/DAY)	IN-OUT (M^3/DAY)
REFERENCE SCENARIO	61,766	25,126	36,640
CLIMATE CHANGE	63,575	24,606	38,969
(B)	**(Reference - CC Scenario) in m^3/day**		-2,329
	Difference in m^3/year		-850,076

The Tagus river shows the opposite results, where the outflow from the aquifer into the river exceeds the inflow from the river into the aquifer system, yet the comparing between scenarios, the river inflow decreases, and the outflow increases under the climate change scenario. This indicates that the decrease in recharge has the same effect on the Tagus river as it induces more inflow to compensate for the volume needed to feed the extraction wells stabilize the steady state of the model. A total volume of 2.5 hm^3/day is reduced from flowing from the aquifer to the Tagus river.

5.4.2 Adaptation Measure

As an adaptation scenario to the future changes in climate patterns, this scenario suggests that all maize cultivated croplands would also cultivate vegetables that would consume less water. It is also assumed that the drip irrigation system has an efficiency of 90%. This assumption leads to a total annual water consumption of 34,546,601 m^3 and a total daily consumption of 94,648 m^3 for irrigation use. The new scenario would decrease the total groundwater extraction by 14%.

Figure 30 shows the results of the groundwater heads and flow direction on the left. In terms of groundwater flow direction patterns and velocity, no significant changes were noticed. Thus, to see the effect on the groundwater drawdown from the reference scenario, the difference in computed head between this scenario and the reference scenario, the PEST calibrated model, is plotted in Figure 30 on the right. The results show a maximum decrease in the drawdown by 0.6 meters at the central south part of the study area, where dense extraction wells exist. This suggests a decrease in the volume of water flowing into the aquifer from the surface water bodies surrounding it, the Tagus and Almonda rivers.

Quantitatively, Table 7 and Table 8 show the total volumetric interaction between the aquifer system and the two rivers, Almonda and the Tagus, for each scenario separately and then the difference between the inflow to and outflow from the aquifer. The net calculation indicates that river Almonda's inflow to the aquifer is greater than the outflow from the aquifer to the river. The net inflow from Almonda decreases by 5,417 m^3/day, saving 8% of the river natural inflow into the aquifer system with a total annual saving of 1.977 hm^3.

As for the Tagus river, the aquifer outflows into it around 4 dm^3 on daily bases in both scenarios with a slight increase in the crop change scenario. At the same time, the inflow from the river to the aquifers system decreases by around 185 m3/day. The net water balance shows a total annual saving of 2.13 hm^3 from the groundwater from the aquifer system that outflows towards the Tagus river.

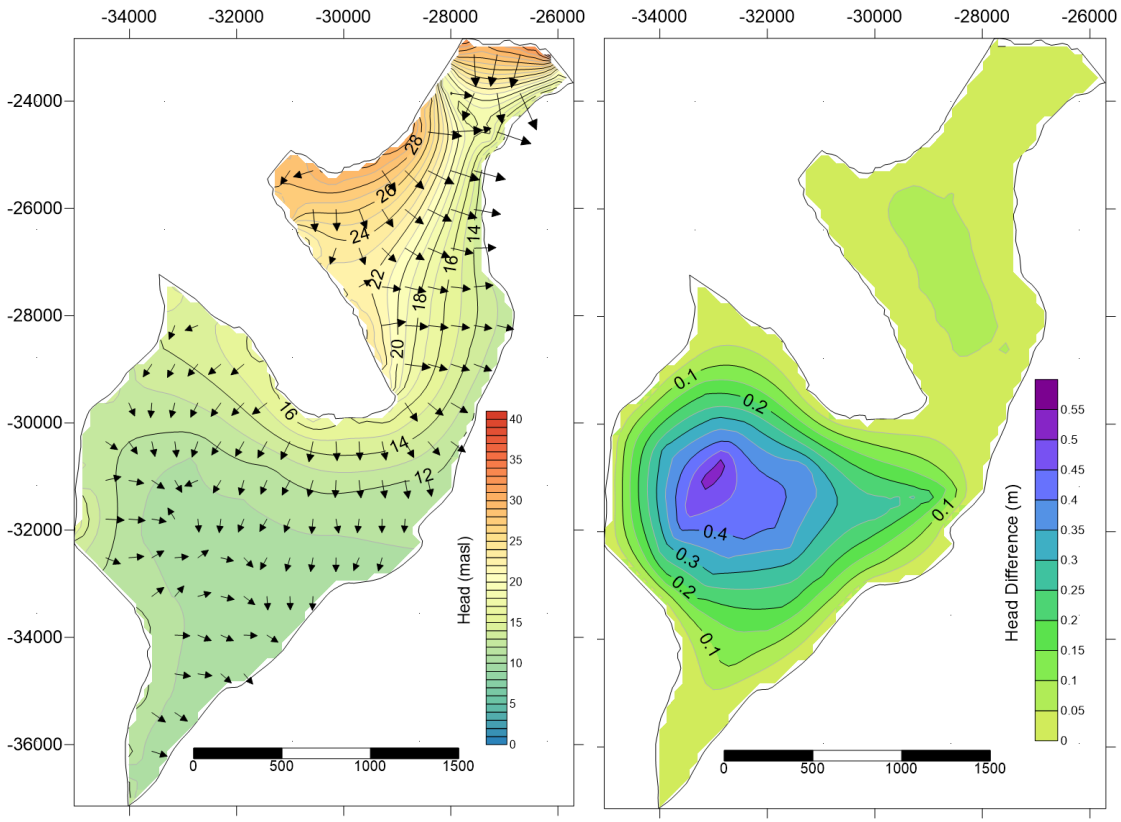

Figure 30: Groundwater Flow (Left) and Difference in the head from the Reference Scenario (Right)

Table 7: Almonda river change in the water budget

	ALMONDA (IN) (M^3/DAY)	ALMONDA (OUT) (M^3/DAY)	IN-OUT (M^3/DAY)
REFERENCE SCENARIO	240,995	176,449	64,546
CROP CHANGE	238,281	179,152	59,129
	Difference in m^3/day		5,417
	Difference in m^3/year		1,977,245

Table 8: Tagus river change in the water budget

	TAGUS (IN) (M^3/DAY)	TAGUS (OUT) (M^3/DAY)	IN-OUT (M^3/DAY)
REFERENCE SCENARIO	34,503	399,136	-364,632
CROP CHANGE	34,319	404,789	-370,470
	Difference in m^3/day		5,838
	Difference in m^3/year		2,130,769

6 Conclusion & Recommendations

This study investigated the potential depletion in the groundwater levels in the Tejo-Sado alluvial aquifer of the Tagus-Sado basin in an intensively irrigated land under uncertain drought conditions, namely the decrease in total precipitation and increase in temperature.

Climate data from the past three decades show an increase in the duration and the frequency of extreme weather events in terms of dry and wet years. Since 2004 droughts have been predominating the extreme events with only one, significant but short, wet event in the year 2010. Because of the very low relief in the topography of the study area, surface runoff is minimal, and infiltration is promoted. Groundwater recharge connection to precipitation is emphasized by the fact that the Tejo-Sado alluvial aquifer is an unconfined aquifer.

Potential evapotranspiration results show an opposite distribution than that of precipitation, where evapotranspiration peaks during summer months and decreases during winter time and vise versa. This leads to the concentration of recharge during the rainy season (i.e. Early autumn and winter months). On the contrary, groundwater extraction for irrigation peaks during summer months, especially July, when the maize, the main crop in the area, is in its peak demand. This supports the assumption that under more frequent dry conditions, the groundwater extraction increases the pressure and dependency on stored groundwater reserve.

Remotely sensed real evapotranspiration data from MODIS proved to be a good tool to use in limited data availability as it gives good estimation compared to values of potential evapotranspiration calculated using local climate data. Although MODIS real evapotranspiration data has a resolution of 500 meters, it proved to be reliable to use for studying a small sty area like the one in hand. The only limitation to the MODIS data is that cloud cover results in areas with no data that must be further corrected before being used in calculating recharge.

The spatial distribution of recharge produced from precipitation and real evapotranspiration data was not conclusive to deduct a correlation between land use and recharge distribution within the study area. That said, only the effect of the Paul Boquilobo natural reserve area could be detected in the recharge distribution, where the evapotranspiration is high due to high vegetation all year long and the existence of a wetland that results in an area of low local recharge.

Groundwater flow modeling results show a general flow direction from the northwest to the southeast. This flow is induced by the assumption that groundwater flow follows the surface topography. The northern part of the study area, identified as zone one, show no change in this main flow except for some local changes close to the constant head boundary that is an effect of the high-resolution DEM used to identify the starting heads of the models. The wide distribution of the extraction wells along with the near proximity to the constant head boundary and the high gradient in topography allowed for the water inflow from the Tejo-Sado right bank aquifer subsystem to compensate for the irrigation demand and resulting in a maximum drawdown of 0.4 meters in this area.

The southern part of the study area, namely zones two & three, show a significant change in the groundwater flow direction toward the center, where the high density of extraction wells exists. The extraction wells induce the flow to go diverge from all directions towards the center, resulting inflows from the Tagus river, Almonda river, and the constant boundary into the aquifer system. A maximum drawdown of 3.6 meters is produced due to this intense extraction backed by the high density of wells in this area. This concludes that the density of the extraction wells is highly influential on the change groundwater depletion.

Quantitative analysis of the interactions between the Tejo-Sado alluvial aquifer subsystem and the bounding rivers, the Tagus and Almonda rivers, along with the bounding aquifer system concludes that 69% of the water inflow into the aquifer system is coming from the adjacent Tejo-Sado right bank aquifer subsystem. That is backed by literature that states that it has a lateral interaction and vertical leakage with the adjacent aquifer system. Rivers are the following contributors by 28% of the total inflow into the aquifer, out of which 88% is flowing from the Almonda river and 12% from the Tagus. Finally, recharge contributes by less than 3% of the total inflow to the aquifer system.

The steady state condition of the groundwater flow model implies a minimal discrepancy between the total inflow and outflow of the system. This ensures that the water is forced to outflow from the system in the form of extraction wells would be compensated by inflows from the boundaries if sufficient. Since the western boundary is defined as a constant head, it acts as an unlimited source of inflow if needed and that explains the predominance of contribution by this boundary.

The sensitivity analysis conducted on the groundwater flow model concludes that the model is most sensitive toward the hydraulic conductivity of the aquifer. Hydraulic conductivity shows sensitivity in terms of both, model performance and water budget while the riverbed conductance shows sensitivity only towards the water budget of the river component of the model, but no significant effect on the model performance.

Automatic parameter estimation using PEST inverse modeling technique proved its ability to enhance the model performance as well as estimating the spatial distribution of the most sensitive parameter. The result of this simulation shows an abrupt change in hydraulic conductivity in the northern part with a north-south orientation. This change follows the same change in the aquifer thickness in this zone. In the southern part, a smoother gradient in the distribution of the hydraulic conductivity is resulting from the natural groundwater flow and the effect of the extraction wells that induces more flow velocity and thus higher calculated hydraulic conductivity.

Following the projections of change in precipitation magnitude by the end of the century in the HadRM GGa2 simulation results in a decrease of 3% in the total annual precipitation in the study area. Although the reduction in the precipitation is not significant, the effect of the change in temperature and consequently the increase in evapotranspiration rates, recharge percentage out of the total annual precipitation decreases from 60% to 24%. This result supports the assumption

that future uncertainty and climate change effect influences the future water recharge of the groundwater resource.

Under the climate change scenario, the inflow from the Almonda river increases while the outflow from the aquifer to the river decrease. Both changes result in an overall change in net balance by 5%. The same effect on the inflow/outflow interaction with the aquifer is noticed but with only 2% change in the total net flow exchange. This supports the assumption that under extremely dry conditions, the groundwater extraction activity induces more inflow from the rivers toward the aquifer compromising the river natural flows.

The suggestion of changing the maize field with other existing vegetables cultivated in the study area, as it indicates market demand, shows a decrease of 14% in the total water demand for agriculture. This scenario implies a recovery in the groundwater heads by a maximum recovery of 0.6 meters in the central south part of the study area. Although the recovery in groundwater head is not significant, this shows that further scenarios of changing crops and decreasing the water demand can be an effective adaptation measure to minimize the effect of coming extreme dry events in the future. Furthermore, this scenario results in saving of 8% of the total net flow exchange between the Almonda river and the aquifer system which helps recover the Almonda natural flow and while saves only 2% of the total net exchange with the Tagus river.

Finally, recommendations for future studies in this study area would be:

- Perform an intensive fieldwork to measure groundwater heads as the national monitoring network (SNIRH) only has one well inside this study area, which is already as indicated in results is very close to the boundary of the aquifer and highly influenced by the boundary condition. This can only be made by getting in contact with local authorities and private landowners as almost all wells were locked when the field visit was conducted during this study.
- Getting more detailed information about the real groundwater extraction rates from each well from the landowners or local authorities.
- Studying the short-term climate variability and the effect of the change in the frequency and magnitude of extreme climate conditions is highly recommended for a more substantial motivation for farmers to take actions in a shorter time period and to help local decision-makers on having a proper management plan for the water resources in the area.
- Gathering more information on the market needs for crops in this region to be able to suggest more realistic changes in the crop to save more water.
- A transient state model for the period of 2016 to 2018 is highly recommended to be studied if the necessary datasets are available from the monitoring network as 2017 was a drought year and studying the transient condition from a normal year to a drought year to a year with significant rainfall events like 2018 would give a complete insight of the

various components of the water balance. This can indicate the lag time between precipitation and change in groundwater heads as an effect of the vadose zone.

7 References

A.P.A. (2012) ‘Plano de gestão da região hidrográfica do tejo. Parte 2 - CARACTERIZAÇÃO E DIAGNÓSTICO DA REGIÃO HIDROGRÁFICA.’, p. 376.

AGROTEJO (2006) *ESTUDO DE IMPACTE AMBIENTAL DO ESTUDO PRÉVIO DO EMPARCELAMENTO RURAL INTEGRADO DE AZINHAGA, GOLEGÃ E RIACHOS RESUMO NÃO TÉCNICO*.

Almeida, C. *et al.* (2000) ‘Sistema Aquífero: Aluviões do Tejo (T7)’, *Sistemas Aquíferos de Portugal Continental*, pp. 649–661.

Canora, C. *et al.* (2015) ‘The Eastern Lower Tagus Valley Fault Zone in central Portugal: Active faulting in a low-deformation region within a major river environment’, *Tectonophysics*. Elsevier B.V., 660, pp. 117–131. doi: 10.1016/j.tecto.2015.08.026.

Cordovil, C. M. d. S. *et al.* (2018) ‘A simplified nitrogen assessment in Tagus River Basin: A management focused review’, *Water (Switzerland)*, 10(4), pp. 1–18. doi: 10.3390/w10040406.

EEA (2016) ‘Use of Freshwater Resources’, 1.

European Union (2006) ‘Directive 2006/118/EC of the European Parliament and of the council of 12 December 2006 on the protection of groundwater against pollution and deterioration’, *Official Journal of the European Union*, 19(L372), pp. 19–31. doi: http://eur-lex.europa.eu/legal-content/EN/TXT/?uri=CELEX:32006L0118.

Fetter, C. W. (2001) *Applied Hydrogeology*, *Applied Hydrogeology*. doi: 0-13-088239-9.

Franke, O. L., Reilly, T. E. and Bennett, G. D. (1987) ‘Definition of Boundary and Initial Conditions in the Analysis of Saturated Ground-Water Flow Systems - An Introduction’, *USGS Techniques of Water-Resources Investigations of the United States Geological Survey*, Book 3, Ap, pp. 1–22.

Freeze, R. a. and Witherspoon, P. a. (1966) ‘Theoretical Analysis of Regional Groundwater Flow : 1. Analytical and Numerical Solutions to the Mathematical Model’, *Water Resources Research*, 2(4), pp. 641–656. doi: 10.1029/WR002i004p00641.

Guttman, N. B. (1998) ‘Comparing the palmer drought index and the standardized precipitation index’, *Journal of the American Water Resources Association*, 34(1), pp. 113–121. doi: 10.1111/j.1752-1688.1998.tb05964.x.

Hubbert, M. K. (1940) ‘The theory of ground-water motion’, *Eos, Transactions American Geophysical Union*. doi: 10.1029/TR021i002p00648-1.

INE (no date) *Instituto Nacional De Estatistica*. Available at: https://www.ine.pt/xportal/xmain?xlang=en&xpid=INE&xpgid=ine_indicadores&indOcorrCod=0005889&contexto=pi&selTab=tab0 (Accessed: 18 November 2018).

Ipcc (2007) *Climate Change 2007: impacts, adaptation and vulnerability: contribution of Working*

Group II to the fourth assessment report of the Intergovernmental Panel, *Genebra, Suíça*. doi: 10.1256/004316502320517344.

McDonald, M. . and Harbaugh, A. W. (1988) 'A modular three-dimensional finite difference ground-water flow model', *Techniques of Water-Resources Investigations, book 6*, p. 588. doi: 10.1016/0022-1694(70)90079-X.

Mendes, M. P. and Ribeiro, L. (2010) 'Nitrate probability mapping in the northern aquifer alluvial system of the river Tagus (Portugal) using Disjunctive Kriging', *Science of the Total Environment*. Elsevier B.V., 408(5), pp. 1021–1034. doi: 10.1016/j.scitotenv.2009.10.069.

Miranda, P. M. A. *et al.* (2002) '20 th Century Portuguese Climate and Climate Scenarios', *Climate Change in Portugal: Scenarios Impacts and Adaptation Measures (SIAM Project)*, pp. 23–83. Available at: http://idl.campus.ciencias.ulisboa.pt/wp-content/uploads/2016/11/Siam1_Clima_0.pdf%0Ahttp://www.dfisica.ubi.pt/~artome/Siam1_Clima_Completo.pdf.

Nash, E. and Sutcliffe, V. (1970) 'PART I- A DISCUSSION OF PRINCIPLES * The problem of determining river flows from rainfall , evaporation , and other factors , occupies a central place in the technology of applied hydrology . It is not only the essential problem of flood forecasting but a', *Journal of Hydrology*, 10, pp. 282–290. doi: 10.1016/0022-1694(70)90255-6.

Running, S. *et al.* (2017) *MODIS 16 User guide*.

Trescott, P. C. (1975) *DOCUMENTATION OF FINITE-DIFFERENCE MODEL FOR SIMULATION OF THREE-DIMENSIONAL GROUND-WATER FLOW*. Available at: https://pubs.usgs.gov/of/1975/0438/report.pdf (Accessed: 28 September 2018).

Vicente-Serrano, S. M., Beguería, S. and López-Moreno, J. I. (2010) 'A multiscalar drought index sensitive to global warming: The standardized precipitation evapotranspiration index', *Journal of Climate*, 23(7), pp. 1696–1718. doi: 10.1175/2009JCLI2909.1.

Vis, G. J. and Kasse, C. (2009a) 'Late Quaternary valley-fill succession of the Lower Tagus Valley, Portugal', *Sedimentary Geology*. Elsevier B.V., 221(1–4), pp. 19–39. doi: 10.1016/j.sedgeo.2009.07.010.

Vis, G. J. and Kasse, C. (2009b) 'Late Quaternary valley-fill succession of the Lower Tagus Valley, Portugal', *Sedimentary Geology*. Elsevier B.V., 221(1–4), pp. 19–39. doi: 10.1016/j.sedgeo.2009.07.010.

Water UK (2012) *W*. Available at: https://www.water.org.uk/publications/policy-positions-and-briefings/hydrological-year (Accessed: 9 November 2018).

Zektser, I. S. and Everett, L. G. (2004) *Groundwater resources of the world and their use*, *IhP Series on groundwater. No. 6*.

Zhou, Y. and Li, W. (2011) 'A review of regional groundwater flow modeling', *Geoscience*

Frontiers. Elsevier B.V., 2(2), pp. 205–214. doi: 10.1016/j.gsf.2011.03.003.

8 Annex

Annex I: Potential Evapotranspiration Calculation

The figures below show the input dataset used to calculate the potential evapotranspiration using the Penman-Monteith equation. The software CROPWAT that is developed by the FAO was used.

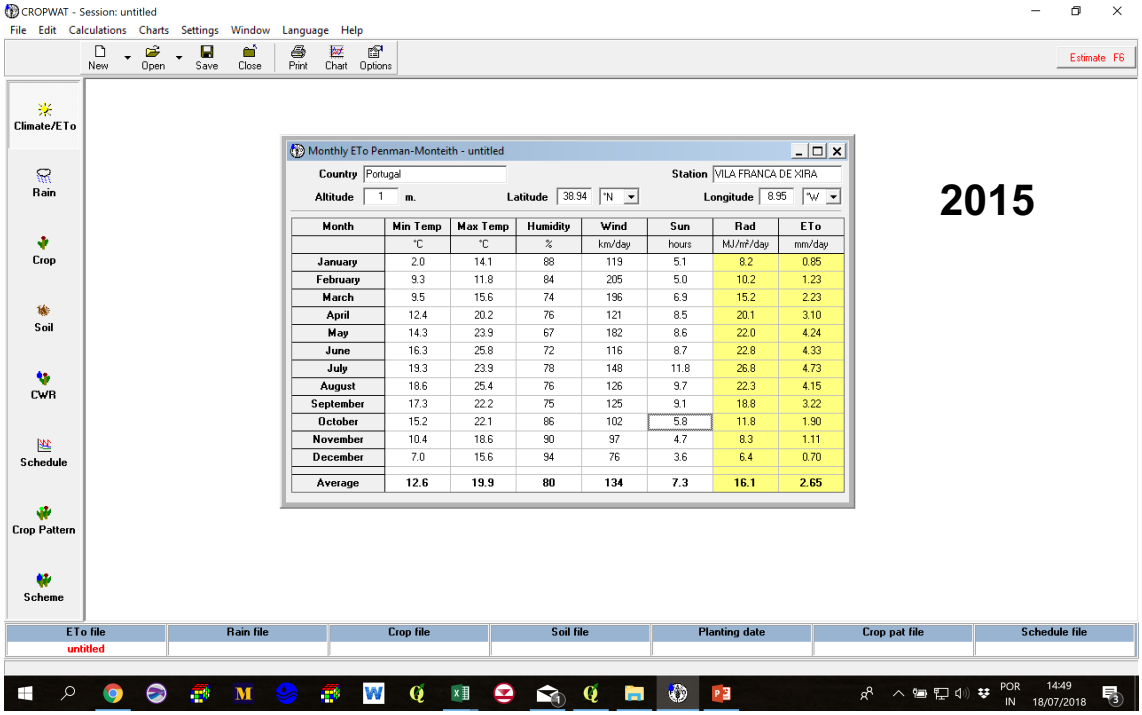

Month	Min Temp	Max Temp	Humidity	Wind	Sun	Rad	ETo
	°C	°C	%	km/day	hours	MJ/m²/day	mm/day
January	2.0	14.1	88	119	5.1	8.2	0.85
February	9.3	11.8	84	205	5.0	10.2	1.23
March	9.5	15.6	74	196	6.9	15.2	2.23
April	12.4	20.2	76	121	8.5	20.1	3.10
May	14.3	23.9	67	182	8.6	22.0	4.24
June	16.3	25.8	72	116	8.7	22.8	4.33
July	19.3	23.9	78	148	11.8	26.8	4.73
August	18.6	25.4	76	126	9.7	22.3	4.15
September	17.3	22.2	75	125	9.1	18.8	3.22
October	15.2	22.1	86	102	5.8	11.8	1.90
November	10.4	18.6	90	97	4.7	8.3	1.11
December	7.0	15.6	94	76	3.6	6.4	0.70
Average	12.6	19.9	80	134	7.3	16.1	2.65

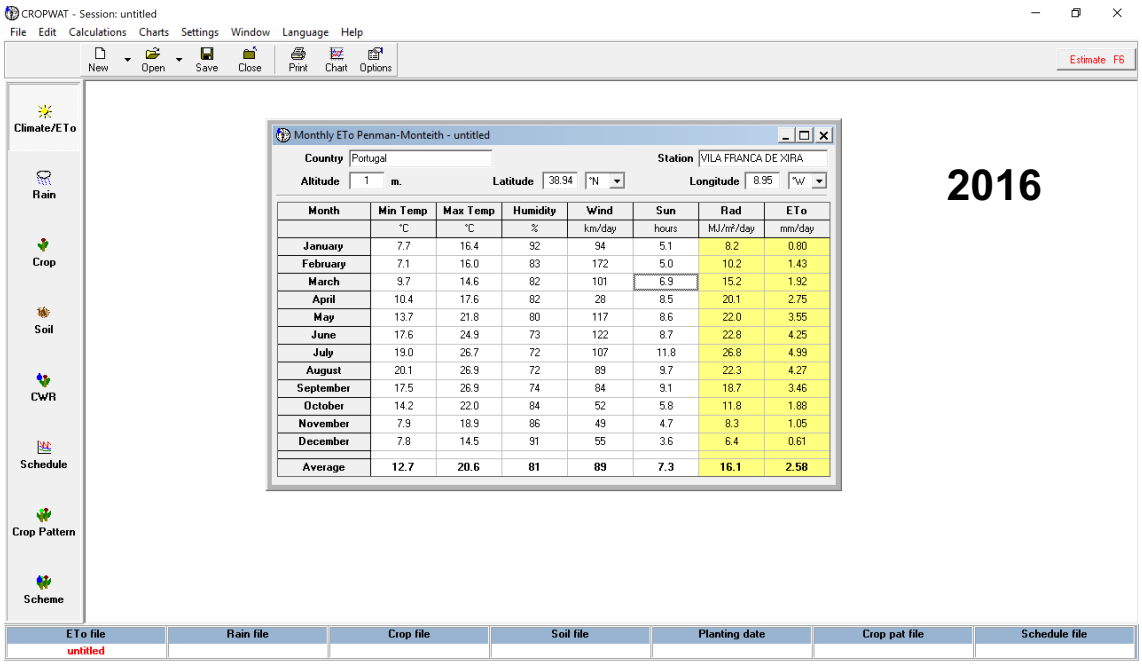

Month	Min Temp	Max Temp	Humidity	Wind	Sun	Rad	ETo
	°C	°C	%	km/day	hours	MJ/m²/day	mm/day
January	7.7	16.4	92	94	5.1	8.2	0.80
February	7.1	16.0	83	172	5.0	10.2	1.43
March	9.7	14.6	82	101	6.9	15.2	1.92
April	10.4	17.6	82	28	8.5	20.1	2.75
May	13.7	21.8	80	117	8.6	22.0	3.55
June	17.6	24.9	73	122	8.7	22.8	4.25
July	19.0	26.7	72	107	11.8	26.8	4.99
August	20.1	26.9	72	89	9.7	22.3	4.27
September	17.5	26.9	74	84	9.1	18.7	3.46
October	14.2	22.0	84	52	5.8	11.8	1.88
November	7.9	18.9	86	49	4.7	8.3	1.05
December	7.8	14.5	91	55	3.6	6.4	0.61
Average	12.7	20.6	81	89	7.3	16.1	2.58

Annex II: Extraction wells pumping rates

Following table shows the pumping rates at each extraction wells in the initial model.

Well # in Pivots	Pumping Rate (m3/d)	Other Wells #	Pumping Rate (m3/d)
1	1088	**1**	1238
2	1242	**2**	1238
3	648	**3**	1238
4	573	**4**	1238
5	1298	**5**	1238
6	601	**6**	1238
7	1540	**7**	1238
8	633	**8**	1238
9	413	**9**	1238
10	292	**10**	1238
11	172	**11**	1238
12	177	**12**	1238
13	166	**13**	1238
14	130	**14**	1238
15	722	**15**	1238
16	317	**16**	1238
17	55	**17**	1238
18	368	**18**	1238
19	340	**19**	1238
20	143	**20**	1238
21	359	**21**	1238
22	372	**22**	1238
23	578	**23**	1238
24	517	**24**	1238
25	361	**25**	1238
26	426	**26**	1238
27	395	**27**	1238
28	526	**28**	1238
29	123	**29**	1238

Well # in Pivots	Pumping Rate (m3/d)	Other Wells #	Pumping Rate (m3/d)
30	105	**30**	1238
31	661	**31**	1238
32	325	32	1238
33	327	**33**	1238
34	341	**34**	1238
35	143	**35**	1238
36	161	**36**	1238
37	344	**37**	1238
38	219	**38**	1238
39	179	**39**	1238
40	394	**40**	1238
41	525	**41**	1238
42	147	**42**	1238
43	470	**43**	1238
44	340	**44**	1238
45	294	**45**	1238
46	494	**46**	1238
47	703	**47**	1238
48	417	**48**	1238
49	68	**49**	1238
50	428	**50**	1238
51	685	**51**	1238
52	113	**52**	1238
53	267	**53**	1238
54	635	**54**	1238
55	353	**55**	1238
56	123	**56**	1238
57	129	**57**	1238
58	267	**58**	1238
59	201	**59**	1238
60	256	**60**	1238
61	247	**61**	1238

Well # in Pivots	Pumping Rate (m3/d)	Other Wells #	Pumping Rate (m3/d)
62	214	**62**	1238
63	175	**63**	1238
64	122	**64**	1238
-	-	**65**	1238
-	-	**66**	1238
-	-	**67**	1238
-	-	**68**	1238

Annex III: Total Water Budget

The tables below show the detailed water budget components at all different stages of the groundwater flow model.

Pre-calibrated Initial Model

Flow Budget for All Zones	
IN	
CONSTANT HEAD	756098.23
WELLS	0.00
RIVER LEAKAGE	109830.86
RECHARGE	35088.78
Total IN	901017.87
OUT	
CONSTANT HEAD	411552.96
WELLS	109289.46
RIVER LEAKAGE	380175.37
RECHARGE	0.00
Total OUT	901017.79
SUMMARY:	
IN - OUT	0.08129632
Percent Discrepancy	9.02E-06

Flow Budget for Zone 1	
IN:	
CONSTANT HEAD	693777.41
WELLS	0.00
RIVER LEAKAGE	10292.04
RECHARGE	13609.25
Zone 2 to zone 1	4310.57
Zone 3 to zone 1	0.00
Total IN	721989.27
OUT:	
CONSTANT HEAD	384660.82
WELLS	23666.35
RIVER LEAKAGE	308064.20
RECHARGE	0.00
Zone 1 to zone 2	5597.91
Zone 1 to zone 3	0.00
Total OUT	721989.28
SUMMARY:	
IN - OUT	-0.01473689
Percent Discrepancy	-2.04E-06

Flow Budget for Zone 2	
IN:	
CONSTANT HEAD	28462.24
WELLS	0.00
RIVER LEAKAGE	978.53
RECHARGE	7928.25
Zone 1 to zone 2	5597.91
Zone 3 to zone 2	22072.73
Total IN	65039.66
OUT:	
CONSTANT HEAD	14488.82
WELLS	14757.34
RIVER LEAKAGE	17507.69
RECHARGE	0.00
Zone 2 to zone 1	4310.57
Zone 2 to zone 3	13975.19
Total OUT	65039.61
SUMMARY:	
IN - OUT	0.051201843
Percent Discrepancy	7.87241E-05

Flow Budget for Zone 3	
IN:	
CONSTANT HEAD	33858.59
WELLS	0.00
RIVER LEAKAGE	98560.30
RECHARGE	13551.27
Zone 1 to zone 3	0.00
Zone 2 to zone 3	13975.19
Total IN	159945.35
OUT:	
CONSTANT HEAD	12403.32
WELLS	70865.76
RIVER LEAKAGE	54603.49
RECHARGE	0.00
Zone 3 to zone 1	0.00
Zone 3 to zone 2	22072.73
Total OUT	159945.30
SUMMARY:	
IN - OUT	0.04483137
Percent Discrepancy	2.8029E-05

Head Observation in m

Obs. Point	Observed Value	Simulated Value	Difference
hed1	10.25	9.48	0.77
hed2	10.22	9.39	0.83
hed3	11.08	11.53	-0.45
hed4	11.13	11.68	-0.55
hed5	19.31	21.15	-1.84

Sum of squared difference	5.176
Mean of Observed Values	12.40
NSE	0.914376155

Manually Calibrated Model

Flow Budget for All Zones	
IN	
CONSTANT HEAD	988740.09
WELLS	0.00
RIVER LEAKAGE	254296.67
RECHARGE	35088.78
Total IN	1278125.54
OUT	
CONSTANT HEAD	497173.64
WELLS	109289.46
RIVER LEAKAGE	671662.66
RECHARGE	0.00
Total OUT	1278125.76
SUMMARY:	
IN - OUT	-0.21871531
Percent Discrepancy	-1.71E-05

Flow Budget for Zone 1	
IN:	
CONSTANT HEAD	912312.88
WELLS	0.00
RIVER LEAKAGE	36303.01
RECHARGE	13609.25
Zone 2 to zone 1	5552.76
Zone 3 to zone 1	0.00
Total IN	967777.91
OUT:	
CONSTANT HEAD	462891.15
WELLS	23666.35
RIVER LEAKAGE	474346.73
RECHARGE	0.00
Zone 1 to zone 2	6873.82
Zone 1 to zone 3	0.00
Total OUT	967778.06
SUMMARY:	
IN - OUT	-0.1556145
Percent Discrepancy	-1.61E-05

Flow Budget for Zone 2	
IN:	
CONSTANT HEAD	34960.42
WELLS	0.00
RIVER LEAKAGE	12.83
RECHARGE	7928.25
Zone 1 to zone 2	6873.82
Zone 3 to zone 2	36284.62
Total IN	86059.94
OUT:	
CONSTANT HEAD	18239.44
WELLS	14757.34
RIVER LEAKAGE	33961.53
RECHARGE	0.00
Zone 2 to zone 1	5552.76
Zone 2 to zone 3	13549.00
Total OUT	86060.07
SUMMARY:	
IN - OUT	-0.12535489
Percent Discrepancy	-0.00014566

Flow Budget for Zone 3	
IN:	
CONSTANT HEAD	41466.78
WELLS	0.00
RIVER LEAKAGE	217980.84
RECHARGE	13551.27
Zone 1 to zone 3	0.00
Zone 2 to zone 3	13549.00
Total IN	286547.89
OUT:	
CONSTANT HEAD	16043.05
WELLS	70865.76
RIVER LEAKAGE	163354.40
RECHARGE	0.00
Zone 3 to zone 1	0.00
Zone 3 to zone 2	36284.62
Total OUT	286547.83
SUMMARY:	
IN - OUT	0.06225407
Percent Discrepancy	2.1726E-05

Head Observation in m

Obs. Point	Observed Value	Simulated Value	Difference
hed1	10.25	10.41	-0.16
hed2	10.22	10.10	0.12
hed3	11.08	11.76	-0.68
hed4	11.13	11.87	-0.74
hed5	19.31	21.14	-1.84

Sum of squared difference	4.424
Mean of Observed Values	12.40
NSE	0.926815273

Climate Change Scenario

Flow Budget for All Zones	
IN:	
CONSTANT HEAD	679873.90
WELLS	0.00
RIVER LEAKAGE	277581.99
RECHARGE	19354.76
Total IN	976810.65
OUT:	
CONSTANT HEAD	299807.93
WELLS	109289.46
RIVER LEAKAGE	567713.86
RECHARGE	0.00
Total OUT	976811.26
SUMMARY:	
IN - OUT	-0.61016055
Percent Discrepancy	-6.25E-05

Flow Budget for Zone 1	
IN:	
CONSTANT HEAD	616298.91
WELLS	0.00
RIVER LEAKAGE	34428.27
RECHARGE	7040.69
Zone 2 to zone 1	4842.77
Zone 3 to zone 1	0.00
Total IN	662610.64
OUT:	
CONSTANT HEAD	275201.80
WELLS	23666.35
RIVER LEAKAGE	357840.80
RECHARGE	0.00
Zone 1 to zone 2	5901.89
Zone 1 to zone 3	0.00
Total OUT	662610.83
SUMMARY:	
IN - OUT	-0.19425589
Percent Discrepancy	-2.93E-05

Flow Budget for Zone 2	
IN:	
CONSTANT HEAD	24276.73
WELLS	0.00
RIVER LEAKAGE	655.32
RECHARGE	4293.48
Zone 1 to zone 2	5901.89
Zone 3 to zone 2	42726.75
Total IN	77854.17
OUT:	
CONSTANT HEAD	11140.99
WELLS	14757.34
RIVER LEAKAGE	34946.77
RECHARGE	0.00
Zone 2 to zone 1	4842.77
Zone 2 to zone 3	12166.51
Total OUT	77854.38
SUMMARY:	
IN - OUT	-0.20398202
Percent Discrepancy	-0.000262

Flow Budget for Zone 3	
IN:	
CONSTANT HEAD	39298.26
WELLS	0.00
RIVER LEAKAGE	242498.40
RECHARGE	8020.58
Zone 1 to zone 3	0.00
Zone 2 to zone 3	12166.51
Total IN	301983.76
OUT:	
CONSTANT HEAD	13465.15
WELLS	70865.76
RIVER LEAKAGE	174926.30
RECHARGE	0.00
Zone 3 to zone 1	0.00
Zone 3 to zone 2	42726.75
Total OUT	301983.97
SUMMARY:	
IN - OUT	-0.21192265
Percent Discrepancy	-7.02E-05

Head Observation in m

Obs. Point	Observed Value	Simulated Value	Difference
hed1	10.25	10.07	0.18
hed2	10.22	9.96	0.26
hed3	11.08	10.91	0.17
hed4	11.13	11.14	-0.01
hed5	18.43	20.72	-2.30

Sum of squared difference	5.4

Automatically Calibrated Model "Reference Scenario"

Flow Budget for All Zones	
IN	
CONSTANT HEAD	675725.63
WELLS	0.00
RIVER LEAKAGE	275498.66
RECHARGE	35088.78
Total IN	986313.07
OUT	
CONSTANT HEAD	301439.25
WELLS	109289.46
RIVER LEAKAGE	575584.38
RECHARGE	0.00
Total OUT	986313.09
SUMMARY:	
IN - OUT	-0.01709419
Percent Discrepancy	-1.73E-06

Flow Budget for Zone 1	
IN:	
CONSTANT HEAD	613959.8116
WELLS	0
RIVER LEAKAGE	34311.55557
RECHARGE	13609.2546
Zone 2 to zone 1	4938.965988
Zone 3 to zone 1	0.00
Total IN	666819.59
OUT:	
CONSTANT HEAD	276313.3053
WELLS	23666.3531
RIVER LEAKAGE	360975.8895
RECHARGE	0
Zone 1 to zone 2	5863.969528
Zone 1 to zone 3	0.00
Total OUT	666819.52
SUMMARY:	
IN - OUT	0.070362687
Percent Discrepancy	1.06E-05

Flow Budget for Zone 2	
IN:	
CONSTANT HEAD	23678.06
WELLS	0.00
RIVER LEAKAGE	191.85
RECHARGE	7928.25
Zone 1 to zone 2	5863.97
Zone 3 to zone 2	43191.68
Total IN	80853.82
OUT:	
CONSTANT HEAD	11274.51
WELLS	14757.34
RIVER LEAKAGE	38159.66
RECHARGE	0.00
Zone 2 to zone 1	4938.97
Zone 2 to zone 3	11723.49
Total OUT	80853.97
SUMMARY:	
IN - OUT	-0.15232348
Percent Discrepancy	-0.00018839

Flow Budget for Zone 3	
IN:	
CONSTANT HEAD	38087.76
WELLS	0.00
RIVER LEAKAGE	240995.25
RECHARGE	13551.27
Zone 1 to zone 3	0.00
Zone 2 to zone 3	11723.49
Total IN	304357.78
OUT:	
CONSTANT HEAD	13851.44
WELLS	70865.76
RIVER LEAKAGE	176448.83
RECHARGE	0.00
Zone 3 to zone 1	0.00
Zone 3 to zone 2	43191.68
Total OUT	304357.71
SUMMARY:	
IN - OUT	0.0648666
Percent Discrepancy	2.1313E-05

Head Observation in m

Obs. Point	Observed Value	Simulated Value	Difference
hed1	10.25	10.28	-0.03
hed2	10.22	10.15	0.07
hed3	11.08	11.06	0.02
hed4	11.13	11.27	-0.14
hed5	19.31	20.74	-1.43

Sum of squared difference	2.082
Mean of Observed Values	12.40
NSE	0.965563517
	6%